Influence of gravity and lift on particle velocity statistics and transfer rates in turbulent vertical channel flow

Cristian Marchioli[1], Maurizio Picciotto[2] and Alfredo Soldati[1,3] *

[1] *Dipartimento di Energetica e Macchine, Università di Udine, Udine 33100, Italy*

[2] *Danieli Research Center, Danieli SpA, Buttrio 33042, Italy*

[3] *Centro Interdipartimentale di Fluidodinamica e Idraulica, Università di Udine, Udine 33100, Italy*

ABSTRACT

The present study reports detailed statistics for velocity and transfer rates of heavy particles dispersed in turbulent boundary layers. The dataset is used to analyze the effects of gravity and lift on particle dispersion and deposition in a systematic way. Statistics were obtained performing Direct Numerical Simulation (DNS) of particle-laden turbulent flow in a vertical channel. Six values for the particle timescale (the particle Stokes number, St) ranging three orders of magnitude were considered to analyze the deposition process as the controlling mechanism was shifting from turbulent diffusion to inertia-moderated crossing trajectories. For the particle timescales examined, gravity and lift do not influence the qualitative behavior of particles even though velocity profiles and deposition coefficients are modified in a non-monotonical fashion, reaching an optimum for $St \geq 25$. Physical mechanisms for the different behavior are discussed. Raw data and statistics obtained from the present DNS are made available at HTTP://CFD.CINECA.IT (mirror site: HTTP://158.110.32.35/DOWNLOAD/DATABASE) and can be used to test simple models and closure equations for multiphase RANS and Large Eddy simulations.

---

*Author to whom correspondence should be addressed. Also affiliated with Department of Fluid Mechanics, CISM, 33100 Udine, Italy. Electronic Mail: soldati@uniud.it.

1. INTRODUCTION

Transport and deposition of solid particles, droplets or aerosols suspended in turbulent gas flow occur in many industrial devices. Examples include filters, risers and downers, pneumatic conveying systems and micro-contamination control facilities. Accurate prediction of particle deposition rate is crucial to design cost-effective industrial processes (Soldati, 2003) and to optimize engineering devices operating with particle-laden flows.

State-of-the-art modelling of particle deposition rate is assessed against experimental data obtained in diverse flow conditions. Considering the variety of test conditions and probing systems, the uncertainty associated with these experimental data is inevitably large, as shown in Fig. 1. This figure is taken from the paper by Young and Leeming (1997) and collects a large number of measurements of particle deposition rate for fully-developed turbulent flow in a circular pipe, as a function of particle response time. Variables are plotted in non-dimensional form (identified by subscript + according to the notation used by Young and Leeming, 1997). The deposition velocity is defined as:

$$V_{dep+} = \frac{J}{\rho_m u_\tau} \ , \tag{1}$$

where J is the deposition mass flux, ρ_m is the mean particle density in the pipe and u_τ is the shear velocity (defined as $u_\tau = \sqrt{\tau_w/\rho}$, where τ_w is the wall shear stress and ρ is the gas density). The non-dimensional particle response time is defined as:

$$\tau_{p+} = \tau_p \frac{u_\tau^2}{\nu} = \frac{\rho_p d_p^2}{18\rho\nu} \frac{u_\tau^2}{\nu} \ , \tag{2}$$

where ν is the kinematic viscosity of the gas, ρ_p is the particle material density and d_p is the particle diameter. The deposition curves of Fig. 1 have been *hystorically* divided into three regimes: the diffusional deposition regime (in which particle transport to the wall may be modelled by gradient diffusion, namely by 'turbulent diffusion' in the core of the flow and Brownian diffusion in the proximity of the wall); diffusion-impaction regime (in which the interaction between particles and turbulent eddies produces an increase of several orders of magnitude in the deposition rate); and the inertia-moderated regime (in which gradient

diffusion takes little or no part since particles can acquire sufficient momentum from the large eddies in the turbulent core to reach the wall directly).

From Fig. 1, uncertainty in the value of V_{dep+} is apparent and the spread of the measurements spans about two orders of magnitude for particles in the diffusion-impaction regime (from $\tau_{p+} = 0.2$ to $\tau_{p+} = 23$). This experimental uncertainty is connected to several reasons. One may be associated to the different circumstances under which each experiment was performed and to the different experimental methods used for sampling and diagnostics. Others are associated with the intrinsic complexity of turbulent transfer phenomena, which are correlated to a wide range of flow scales depending on the different mechanisms governing the interaction between particles and turbulent structures. Due to this complexity, most practical flows are commonly simulated using simplified models (Elghobashi and Abou-Arab, 1983; Soldati and Andreussi, 1996; Young and Leeming, 1997; Sergeev et al., 2002 to name a few). Our simulations were motivated by the need for reliable and accurate sets of data that can be used to validate closure relations of either theoretical or engineering models (e.g. Reynolds-averaged two-fluid Eulerian models). The need for this type of data can be extended also to commercial softwares for computational fluid dynamics. In our experience, these softwares, usually exploited for high-Reynolds-number flows in complex geometries, in the *RANS mode* fail predictions of multiphase flows due to the lack of appropriate physical models for particle dispersion, resuspension and deposition. In this paper, data are provided in the form of velocity and deposition statistics for the dispersed phase.

Another goal is to evaluate quantitatively the effects of gravity and lift on particle dispersion, since these effects may become as important as those due to particle inertia and to fluid turbulence. Previous experimental (Friedlander and Johnstone, 1957; Liu and Agarwal, 1974; Kaftori et al., 1995a, 1995b; Niño and Garcia, 1996; Righetti and Romano, 2004) and computational studies (McLaughlin, 1989, Brooke et al., 1994; Uijttewaal and Oliemans, 1996; van Haarlem et al., 1998; Zhang and Ahmadi, 2000; Narayanan et al., 2003; Marchioli et al., 2003) showed that particle distribution in wall-bounded turbulent flows is made highly non-homogeneous by the coupled action of turbulence and particle inertia. However, particles under the influence of a potential field (e.g. gravity) become disengaged from fluid

turbulence and rapidly travel through fluid eddies sampling flow velocities that are more and more decorrelated. The well-known crossing-trajectory effect (Csanady, 1963; Wells and Stock, 1983; Maxey, 1987) is a reasonable explanation for this behavior.

In homogeneous turbulence, the crossing-trajectory effect is known to control the gravitational settling of heavy particles: these particles fall from one eddy to another at a rate faster than the average eddy-decay rate, lose velocity correlation more rapidly and disperse less (Wells and Stock, 1983). In the present study, which is part of a broader effort (as documented in Soldati, 2005), we use DNS to single out the effect of gravity for the case of non-homogeneous turbulence. We will also analyze the inclusion of the lift force term in the particle equation of motion. The influence of the lift force in determining the build-up of particle concentration in the viscous sublayer is modulated by gravity, which acts to increase/decrease the slipd velocity between particles and fluid: thus, the model chosen to reproduce the effect of lift may have a considerable impact on the prediction of particle deposition.

To the best of our knowledge, very few studies are available which analyze in a systematic way the effects of gravity and/or lift on particle transfer and deposition. In addition, analyzes are not systematic and report data which are difficult to compare. For our purposes, the reference work is the numerical experiment by Uijttewaal & Oliemans (1996), where both effects for inertial particles in vertical pipe flow were considered. It was shown that, when drag and gravity are the only forces acting, particles with response time larger than the integral timescale of near-wall turbulence structures have higher deposition rate in upward flow (where gravity acts against the mean flow) than in downward flow (where gravity acts along the mean flow direction) or flow with zero gravity. Similar results were obtained by Zhang and Ahmadi (2000) for particles dispersed in channel flow.

Regarding the lift force, Uijttewaal and Oliemans (1996) modelled the corresponding term in the particle equation of motion using a simplified expression valid for a particle in a shear flow away from walls (Saffman, 1965; McLaughlin, 1991). As demonstrated by subsequent studies (see Wang et al., 1997 and Kurose and Komori, 1999 among others), this model is inaccurate for deposition near solid boundaries and high particle Reynolds numbers: more

general derivations are thus needed to improve the accuracy of predictions.

Starting from this background, we will focus on a fully-developed turbulent flow in a vertical channel. The present study adds to works cited above since it was designed to be a homogeneous source of data covering a broad range of situations and providing: (i) accurate numerical procedure (fully-resolved pseudo-spectral DNS); (ii) wide spectrum of particle timescales; (iii) larger particle samples to ensure adequate statistical convergence of the results; (iv) accurate particle statistics. In particular, we have chosen values of the particle time scale ranging from the diffusion-impaction regime to the inertia-moderated regime. This choice enabled us to discriminate among the different mechanisms of particle dispersion and is justified in the frame of previous analyzes (Picciotto et al., 2005a; 2005b) which showed that this range includes particles that are the most responsive to the boundary layer flow structures. For each particle timescale, particle samples ten times larger than those used by Uijttewaal and Oliemans (1996) were considered.

2. METHODOLOGY

2.1. Channel Flow Simulation

Particles are dispersed in a pressure-driven fully-developed turbulent flow of air, assumed to be incompressible and Newtonian (density $\rho = 1.3\ kg\ m^{-1}$, kinematic viscosity $\nu = 15.7{\times}10^{-6}\ m^2 s^{-1}$). The flow is bounded by two infinite flat parallel walls with origin of the coordinate system located at the channel centerline and the x, y and z axes pointing in the streamwise, spanwise and wall-normal directions respectively. Periodic boundary conditions are imposed on the fluid velocity field both in x and y; no-slip boundary conditions are enforced at the walls. We assume that particle number density and particle size are both small, and that there is no feedback of the particles onto the gas flow.

Three different flow configurations were considered: no gravity, vertical downward and vertical upward, hereinafter labeled as G_0, G_d and G_u respectively (see Fig. 2). The G_0 configuration may be of interest for space-type applications which require accurate measurements of turbulence-induced preferential distribution of particles under micro-gravity

conditions.

The flow field was calculated by integrating the mass and momentum balance equations in dimensionless form (obtained using the channel half-width, h, and the shear velocity, u_τ):

$$\nabla \cdot \mathbf{u} = 0, \tag{3}$$

$$\frac{\partial \mathbf{u}}{\partial t} = -\mathbf{u} \cdot \nabla \mathbf{u} + \frac{1}{Re} \nabla^2 \mathbf{u} - \nabla p + \delta_{1,i}, \tag{4}$$

where $\mathbf{u}$ is the dimensionless fluid velocity vector, p is the fluctuating kinematic pressure, $\delta_{1,i}$ is the mean dimensionless pressure gradient that drives the flow and $Re_\tau = u_\tau h/\nu$ is the shear Reynolds number. Eqs. 3 and 4 are solved using a pseudo-spectral method. Details of the numerical method can be found elsewhere (Lam and Banerjee, 1992).

Calculations are performed on a computational domain of $1885 \times 942 \times 300$ wall units in x, y and z discretized with $128 \times 128 \times 129$ nodes. The Reynolds number of the flow is $Re = 2100$ based on the bulk velocity $u_b = 1.65\ m\ s^{-1}$. The corresponding shear Reynolds number is $Re_\tau = 150$, which gives $u_\tau = 0.11775\ m\ s^{-1}$: the rationale for considering a single value is that, in small Reynolds number wall turbulence and in the case of heavy particles, the Reynolds number of the flow has little effect on particles and particle timescale normalized to wall variables may be used as the representative Stokes number. Current direct numerical simulations at higher Reynolds number ($Re_\tau = 360$, see Portela et al., 2002) do not show strong differences. Effects of the Reynolds number might perhaps be observable for higher shear Reynolds numbers which, however, are currently beyond the capabilities of our laboratory.

The time step used is $\Delta t^+ = 0.045$ in wall time units: the statistics of the flow field (some of which are shown in Section 3.2) have been presented before in Giusti et al. (2005) and were collected up to $t^+ = 1192$ and are consistent with previous simulations (Kim et al., 1987; Lyons et al., 1991).

2.2. Discrete Particle Tracking

Pointwise, rigid, spherical particles are injected into the flow at concentration low enough to neglect particle collisions. The effect of particles onto the turbulent field is also neglected

(one-way coupling assumption). Even though the accumulation process can produce local peaks of particle number density near the wall, it was shown that turbulence structures seem to modify only from a quantitative viewpoint (Kaftori et al., 1995a; 1995b; Pan and Banerjee, 1996).

Particle motion is described by a set of ordinary differential equations for particle velocity and position at each time step. For particles much heavier than the fluid ($\rho_p/\rho \simeq 769$), Elghobashi and Truesdell (1992) have shown that the only significant forces are Stokes drag and buoyancy and that Basset force can be neglected being an order of magnitude smaller. Brownian diffusion becomes important for particles smaller than those considered in this study (Soltani and Ahmadi, 1995) and was also neglected.

For the purposes of the present analysis, we decided to include the effect of the lift force in the equations of particle motion. Uijttewaal & Oliemans (1996), Rouson & Eaton (2002), and Marchioli et al. (2003) showed that, for small particles, the lift force term becomes formally of the same order in particle radius as other terms we neglected in the more complete equation of motion derived by Maxey & Riley (1983). In this situation, the lift force is small compared to the particle drag in the same direction and modifies slightly deposition statistics from a quantitative (yet not qualitative) viewpoint. For larger particles, however, the lift force may have non-negligible effects on the rate of particle accumulation near the wall, particularly in presence of a solid boundary (Wang and Squires, 1996).

With the above simplifications the following Lagrangian equation for the particle velocity is obtained (Maxey and Riley, 1983):

$$\frac{d\mathbf{v}}{dt} = -\frac{3}{4}\frac{C_D}{d_p}\left(\frac{\rho}{\rho_p}\right)|\mathbf{v}-\mathbf{u}|(\mathbf{v}-\mathbf{u}) + C_L\frac{\rho}{\rho_p}\left[(\mathbf{u}-\mathbf{v})\times\omega\right] + \left(1-\frac{\rho}{\rho_p}\right)\mathbf{g}\ . \tag{5}$$

In Eq. 5, $\mathbf{v}$ is particle velocity, $\mathbf{u}$ and ω are fluid velocity and vorticity at particle position, and d_p is particle diameter. $C_D = \frac{24}{Re_p}(1+0.15Re_p^{0.687})$ is the corrected Stokes drag coefficient, which depends on the particle Reynolds number $Re_p = d_p|\mathbf{v}-\mathbf{u}|/\nu$: the correction for C_D is necessary when Re_p does not remain small.

In the lift force term, the coefficient C_L is a function of the particle Reynolds number and of the dimensionless parameter $Sr_p = |(\mathbf{u}-\mathbf{v})\times\omega|\, d_p/|\mathbf{u}-\mathbf{v}|^2$. We calculated C_L as

(McLaughlin, 1991, Kurose and Komori, 1999; Giusti et al., 2005):

$$C_L \begin{cases} = C_{L_{McL}} = \left[5.816 \left(\frac{Sr_p}{2\ Re_p}\right)^{0.5} - 0.875\frac{Sr_p}{2}\right] \frac{3}{4\ Sr_p}\frac{J(\epsilon)}{2.255} & for\ Re_p < 1\ , \\ = C_{L_{McL}}\frac{5-Re_p}{4} + C_{L_{KK}}\frac{Re_p-1}{4} & for\ 1 < Re_p < 5\ , \\ = C_{L_{KK}} = \left[K_0\ \left(\frac{Sr_p}{2}\right)^{0.9} + K_1\ \left(\frac{Sr_p}{2}\right)^{1.1}\right] \frac{3}{4\ Sr_p} & for\ Re_p > 5\ . \end{cases} \quad (6)$$

In Eq. 6, $C_{L_{McL}}$ indicates the coefficient calculated using the formula by McLaughlin (1991). The function $J(\epsilon)$ is also reported in McLaughlin (1991), the variable ϵ being defined as $\epsilon = (Sr_p/Re_p)^{0.5}$. $J(\epsilon)$ is a correction factor added by McLaughlin (1991) to the expression of the lift force model reported by Saffman (1965) to extend its validity to situations where the hypothesis of negligible Re_p is not ensured. The coefficient $C_{L_{KK}}$ is calculated as in Kurose and Komori (1999), K_0 and K_1 being tabulated values depending on Re_p. The coefficient C_L, used to calculate the lift force acting on particles, is set equal to $C_{L_{McL}}$ for low particle Reynolds numbers ($Re_p < 1$) and equal to $C_{L_{KK}}$ for high particle Reynolds numbers ($Re_p > 5$). Following Giusti et al. (2005), a linear interpolation between the coefficients $C_{L_{McL}}$ and $C_{L_{KK}}$ is used to calculate C_L for intermediate values of particle Reynolds number ($1 < Re_p < 5$).

The last term on the R.H.S. of Eq. 5 includes the gravitational acceleration in vector form, $\mathbf{g}$. Gravity is introduced in this study by giving $\mathbf{g}$ a non-dimensional absolute value $g^+ = g\nu/u_\tau^3 = 0.0943$.

A Lagrangian particle tracking routine coupled with the DNS code was developed to calculate particles paths in the flow field. The routine uses sixth-order Lagrangian polynomials to interpolate fluid velocities at particle position; with this velocity the equations of particle motion are advanced in time using a fourth-order Runge-Kutta scheme. The performance of the interpolation scheme is comparable to that of spectral direct summation and to that of an hybrid scheme which exploits sixth-order Lagrangian polynomials in the streamwise and spanwise directions and Chebychev summation in the wall-normal direction. For the simulations presented here, six sets of 10^5 particles were considered, spanning three orders of magnitude of their response time, τ_p. Here, the non-dimensional particle response time,

obtained using wall variables as in Eq. 2, corresponds to the particle Stokes number:

$$St = \tau_{p+} = \frac{\tau_p u_\tau^2}{\nu} \ . \tag{7}$$

In the present study, we have selected $St = 0.2$, 1, 5, 15, 25 and 125. Table 1 summarizes the complete set of parameters relevant to the simulations of particle dispersion, including the non-dimensional values of the stationary average settling velocity of the particles, V_s^+, and the corresponding values of the particle Reynolds number, Re_p^+. Table 1 groups a total number of 36 cases (6 particle sets in 3 flow configurations with and without lift), which represent a complete and homogeneous source of data covering a large target parameter space.

At the beginning of the simulation, particles are distributed homogeneously over the computational domain and assume a uniform distribution. Their initial velocity is set equal to that of the fluid in the particle initial position. Upon release, particles need to adapt to the flow and to forget their initial conditions: typically, it takes a few particle response times before reliable statistics can be gathered. Statistics were computed over the interval $\Delta t^+ = 450$ starting at time $t^+ = 742$, which corresponds to nearly six non-dimensional response times of the larger particles ($St = 125$).

Periodic boundary conditions are imposed on particles in both streamwise and spanwise directions. Elastic reflection is applied when the particle centre is less than a distance $d_p/2$ from the wall. Even in case of elastic reflection the behavior of the dispersed phase is characterized by a long transient during which wallward net fluxes of particles occur (Portela et al., 2002; Picciotto et al., 2005b). At steady state, the flux of particles toward the wall must be balanced by the flux in the opposite direction returning the particles to the bulk of the flow. However, it is not obvious that a non-trivial statistically steady state can be achieved for all particle sizes. In the case of large particles, whose mean free path is comparable with or larger than the size of near-wall region, a mechanism for such a flux can be provided by elastic wall collision of particles having large wall-normal velocity. In the case of particles with small mean free path, the interaction with the wall will resemble an absorbing-wall condition rather than an elastic-bouncing condition (Portela et al., 2002),

and the statistically steady state might be trivial: empty bulk flow and densely populated near-wall region.

Note that the data sets obtained assuming perfectly reflecting walls can be used to extract subsets of data for the case of perfectly absorbing walls simply by tagging time and location of the particle upon impact.

2.3. Calculation of Statistics

The aim of this study is to provide accurate statistics for benchmarking and model validation. We will be mostly interested in providing statistics for particle velocities. However, since particle distribution is evolving and will require long times to reach steady state (Portela et al., 2002), statistics influenced by particle distribution will not be at steady state. Elaborating, we have $T_l < \Delta t^+ << T_L$, where $T_l \simeq \tau_p$ represents the time scale taken by the particle to reach a condition of local equilibrium with the surrounding fluid and T_L represents the time scale required to reach a statistically-steady particle concentration. Statistics like particle concentration and wall-normal particle velocity (which will be shown in Sections 3 and 4) scale with T_L and simulation times much longer than Δt^+ are thus required to compute their steady-state values. Statistics like the streamwise particle velocity, the particle rms velocity components and the deposition coefficient (shown in Sections 3 and 4 as well) scale with T_l: for these quantities, simulation times comparable to Δt^+ are sufficient to compute steady-state values.

3. EFFECTS OF GRAVITY ON PARTICLE STATISTICS

This section features some of the statistics obtained from the simulations with different gravity set ups and no lift force acting on particles. These statistics are the most relevant to single out the effect of gravity on the processes of particle dispersion, deposition and preferential distribution.

3.1. Particle Number Density Profiles

To quantify the macroscopic evolution of particle accumulation and deposition at the wall, we have monitored the time behavior of the particle number density, n_p, as function of the wall-normal coordinate, z^+. Starting from the initial uniform distribution of particles, number density profiles were computed at different times of the simulation binning the channel height into $N_b = 129$ slabs through Chebyshev polynomials and counting the proportion of particles that fell within each slab, i.e. by averaging over the streamwise and spanwise directions. Fig. 3 shows the instantaneous particle number density profiles at times $t^+ = 675$ (Figs. 3a to 3m, left column) and $t^+ = 1125$ (Figs. 3b to 3n, right column). For convenience, particle number density is normalized by its initial value. Symbols are as follows: plus signs refer to channel flow without gravity (case G_0), black boxes refer to vertical downward flow (case G_d) and empty circles refer to vertical upward flow (case G_u). A logarithmic scale is used to expand the near-wall region and to capture the different behavior of particle transfer. Consider that, in dimensionless wall units (see Table 1), particles of the five dimensions investigated touch the wall when their center is one particle radius far from the wall, namely at $z^+ = 0.034$, $z^+ = 0.0765$, $z^+ = 0.171$, $z^+ = 0.293$, $z^+ = 0.3825$ and $z^+ = 0.855$ respectively (the last point of the plot). For the larger particles, these impact distances may encompass several grid points (five in the case of the $St = 125$ particles).

As already observed by Picciotto et al. (2005b) for the same flow and particle parameters, near-wall accumulation in the no-gravity configuration (when only drag acts on particles) builds up over time due to particle interaction with the local turbulent flow structure. Profiles develop a peak within one viscous unit from the wall and the peak value, indicated as n_p^{max} hereinafter, increases with particle inertia up to $St = 25$: at this Stokes number, particles respond maximally to the near-wall flow structures and the largest concentration at the wall occurs (Figs. 3i and 3l). A further increase of particle inertia corresponds to a smaller concentration at the wall (see Figs. 3m and 3n, relative to the $St = 125$ particles). This trend is qualitatively maintained when gravity is applied in the two vertical flow configurations; quantitative differences in the profiles become significant only for the larger

particles and depend on the orientation of gravity with respect to the mean flow.

Profiles shown in Fig. 3 were computed under a statistically-developing condition for the particle concentration: typically, the deposition process is very slow and a considerable amount of time is required to achieve a stationary distribution of particles over the channel cross-section. The rate of convergence toward a stationary particle distribution is visualized in Fig. 4, where the time-behavior of n_p^{max} (normalized to its initial value) is shown for particles with different inertia. The steep monotonic increase of n_p^{max} indicates that the deposition process is actually far from a statistically-steady state (Portela et al., 2002). Profiles do not differ significantly from each other for the smaller particles (Figs. 4a-c) while interesting differences (both qualitative and quantitative) are observed for the larger particles. After an initial transient of about 600 t^+, gravity reduces the concentration peak of the $St = 15$ and $St = 25$ particles in both upflow and downflow (Figs. 4d and 4e, respectively). In contrast, gravity increases the concentration peak of the $St = 125$ particles in upflow, but has little effect in downflow (Figs. 4f). Since no lift force model is applied in these cases, differences in particle behavior can be established solely by particle-turbulence interaction in combination with the crossing-trajectory effect.

3.2. Statistics of Particle Velocity

In the previous paragraph we quantified the effect of gravity on particle accumulation at the wall. Here, we will analyze the statistics of particle velocity for each flow configuration with no lift force model. A similar statistical analysis, yet focused on the effect of particle inertia, can be found in Picciotto et al. (2005a). In that work, a comparative study of particle and fluid velocity statistics for channel flow without gravity was proposed to show that the inertial filtering causes a lag in the particle-to-fluid relative velocity in the streamwise direction and affects particle wallward drift velocity in the wall-normal direction. Of course, applying gravity introduces further modifications to the mean velocity profiles.

To compute the mean particle velocities shown in this section the following steps were taken. First, we divided the channel height into N_b wall-parallel bins. The b^{th} bin has

thickness:

$$\Delta z_b^+ = \frac{Re_\tau}{2}\left[1 - cos\left(\pi \cdot \frac{b-1}{N_b - 1}\right)\right] \ ,$$

which is equal to the wall-normal distance between two neighbouring grid points and decreases toward the wall to provide a relatively large number of small bins where the flow conditions change rapidly. Then, at each time step we determined the bin containing the particle and we computed the local instantaneous mean particle velocity within each bin. Finally, we averaged the instantaneous values over time from $t^+ = 742$ to $t^+ = 1192$. Fig. 5 shows the mean particle streamwise velocity, v_1^+, as a function of the wall-normal coordinate, z^+, for each particle timescale and each gravity set up. Also shown is the mean streamwise velocity of the fluid (solid line). Modifications to the particle velocity profiles gradually appear as particle inertia increases. While the profiles for the smaller particles overlap almost perfectly (Figs. 5a-b), those relative to the $St = 5$ particles (Fig. 5c) are slightly shifted from each other: when gravity is applied, v_1^+ decreases in upflow (G_u, open circles) and increases in downflow (G_d, black boxes). As expected, this trend is enhanced for the larger particles (Figs. 5d-f) and has consequences for the direction of the lift force, whose effect on particles will be analyzed in Section 4. On average, particles in upflow lag the fluid - close to the wall they actually fall down - so that the lift force is directed toward the channel centerline leading to a decreased deposition; particles in downflow lead the fluid and they are likely to be propelled toward the wall contributing to an increased deposition.

Fig. 6 shows the profiles of the mean particle wall-normal velocity, v_3^+, as a function of the wall-normal coordinate, z^+. Symbols are the same as in Fig. 4. Recall that the wall-normal velocity is directed toward the wall if negative and away from the wall if positive. When gravity is omitted from the equation of motion (case G_0), particles are characterized by a mean drift velocity directed toward the wall which increases up to $St = 25$ and then decreases (Picciotto et al., 2005b). Applying gravity affects slightly the smaller particles as shown in Figs. 6(a-c): v_3^+ is characterized by relatively small values, that produce scattered data points and make the curves a bit ragged. Differences become more relevant and interesting to comment for the larger particles. The drift velocity for the $St = 15$ and the $St = 25$

particles (Figs. 6d and 6e, respectively) tends to decrease even though profiles maintain their qualitative behavior. From a quantitative viewpoint, the drift velocity of the $St = 25$ particles is smaller in downflow than in upflow, where more slight reductions occur for $30 < z^+ < 100$. Modifications on the wall-normal velocity profiles of the $St = 125$ particles (Fig. 6f) are both quantitative and qualitative. As already mentioned, v_3^+ remains negative - i.e. directed toward the wall - throughout the channel height when gravity is not applied, and the corresponding profile develops a single peak not far from the wall (roughly at $z^+ \simeq 40$ in wall units). When gravity is applied (cases G_d and G_u), profiles acquire a wavy shape and v_3^+ becomes positive - i.e. directed away from the wall - outside the buffer layer, where a further local peak is observed. In downflow (black squares), the region of positive v_3^+ is much larger than the region of negative v_3^+, the cross-over occurring at $z^+ \simeq 50$. In upflow (open circles), the region of negative v_3^+ is predominant as the cross-over point shifts toward the channel centerline, at $z^+ \simeq 100$.

The presence of mean particle drift velocities oriented in opposite directions can be explained in connection with the mechanisms governing particle transfer to the wall or away from the wall. It is not our object to focus on these mechanisms and the reader is referred to the paper by Marchioli and Soldati (2002) for further details. Here, we just recall that particle transfer is controlled by two types of momentum-carrying events, both displaying strong spatial coherence: in-sweeps of high-momentum fluid directed toward the wall and ejections of low-momentum fluid directed away from the wall. On average, particles are either driven to the wall by the in-sweeps or entrained away from the wall by the ejections; the efficiency of this process depends on the presence of particles in regions where the transfer mechanisms can entrain them (Marchioli and Soldati, 2002). In the specific case of downflow, particles lead the fluid (see Figs. 5d 5e and 5f for instance) and move along straight paths stepping from one eddy to another. During this motion, particles tend to occupy flow regions of high streamwise velocity, where ejections are more likely to occur. In contrast, particles in upflow lag the fluid and preferentially sample regions of low streamwise velocity, which typically indicate the occurrence of in-sweeps.

To complete the statistical analysis of particle motion under the influence of gravity, it

is useful to evaluate the particle turbulence intensities. Figs. 7 and 8 show the root mean square (rms) of particle velocity along the streamwise direction, $v_1^{+,rms}$, and the wall-normal direction, $v_3^{+,rms}$, respectively. Profiles for the fluid are also shown (dashed lines). Comparing both figures, we observe that: (i) particle velocity rms is higher than that of the fluid in the streamwise direction (with the exception of the $St = 125$ particles) and lower in the wall-normal direction, this behavior being mostly due to particle inertia rather than gravity as explained in Portela et al. (2002) and in Picciotto et al. (2005a); (ii) the rms profiles overlap almost perfectly for the smaller particles ($St = 0.2$, 1 and 5) and the inclusion of gravity appears significant only for $St \geq 15$ producing quantitative changes which do not modify particle behavior from a qualitative viewpoint.

Focusing on the streamwise velocity fluctuations (Fig. 7), we observe that all profiles develop a peak at $z^+ \simeq 15$, which experiences a monotonic increase up to $St = 25$ (Figs. 7a-e) followed by a decrease for the $St = 125$ particles. This behavior can be better appreciated in the close-up view included in each diagram. As shown in Fig. 7f, these particles are affected by gravity in different ways depending on the flow configuration: in upflow, their streamwise velocity fluctuations are always smaller than in the no-gravity flow and reach the peak value closer to the wall (at $z^+ \simeq 5$ roughly); in downflow, smaller fluctuations occur only outside the buffer layer ($z^+ > 30$) or in proximity of the viscous sublayer ($z^+ < 10$) whereas the peak value shifts away from the wall. In contrast, gravity appears to enhance the inertial filtering of particle wall-normal velocity fluctuations (Fig. 8), which are most important for transport, concentration distribution and deposition at the wall. This filtering effect is particularly evident in the center of the channel and becomes more pronounced as particle inertia increases, yet it does not seem to depend on the direction of gravity.

Particle velocity profiles shown in Fig. 5 give rise to high particle Reynolds numbers, which depend on the wall-normal direction. Fig. 9 shows the behavior of the particle Reynolds number, Re_p, along the wall-normal ccordinate, z^+, for all flow configurations and all particle sets considered. For high values of Re_p, the validity of the lift force model used in Eq. 5 should be ensured by the coefficient of Eq. 6. However, Re_p depends highly on the particle response time, τ_p (Uijttewaal and Oliemans, 1996). For instance, particles with

large response time will have $Re_p > 1$. In this case, due to the non-linear drag coefficient accounting for high Re_p (see Eq. 5), the actual particle response time will be smaller than τ_p: $Re_p = 10$ already leads to a 40% reduction.

Applying gravity causes an increase in the velocity difference between particles and fluid due to sedimentation of the large particles resulting in an even larger Re_p. Fig. 9 shows that this increase occurs throughout the channel height for all particle sizes. The increase of Re_p for downflow (case G_d) is smaller than for upflow (case G_u) in the center of the channel. This happens because, in this region, particles in downflow lead the fluid while particles in upflow lag the fluid with an even higher velocity. For downflow, the near-wall increase of Re_p results from an increased velocity difference in the streamwise direction and is larger than in upflow, where the smaller upward particle velocities correspond better to the small near-wall fluid velocities.

A detailed statistical analysis of particle motion was also provided by Uijttewaal and Oliemans (1996) to characterize particle deposition in vertical pipe flows. However, comparison with the present results is rather difficult due to differences in the shear Reynolds numbers of the flow ($Re_\tau = 360$, higher than in our simulations) and in the particle Stokes numbers (some results are shown for $St = 5120$ particles only).

3.3. Particle Deposition Rates

The tendency of particles to deposit at the wall produces the concentration profiles shown in Fig. 3. Here we will examine the rate at which particles deposit, also known as deposition velocity. Virtually all the experimental data on the deposition rate have been obtained in turbulent pipe flow. However, because deposition is mainly controlled by the near-wall turbulence, calculations for channel flow, non-dimensionalised with respect to wall variables, give similar results to pipe flow and provide a suitable tool for model validation.

Following Cousins and Hewitt (1968), the deposition rate of non-interacting particles is proportional to the ratio between the mass flux of particles at the deposition surface, J, and the mean bulk concentration of particles, C. According to this definition, the constant

of proportionality, defined as the deposition coefficient k_d, can be calculated through the following turbulent transport equation:

$$J = -k_d \cdot C \ . \tag{8}$$

Given the initial number N_0 of particles released in the channel, we discretized the non-dimensional flux of particles, J^+, and mean bulk concentration, C^+, as follows:

$$J^+ = \frac{1}{A_d^+} \cdot \frac{dN_{dep}(t^+)}{dt^+} = \frac{1}{L^+W^+} \cdot \frac{\Delta N_{dep}(t^+)}{\Delta t^+} \ , \tag{9}$$

$$C^+ = \frac{N_0 - N_{dep}(t^+)}{V^+} = \frac{N_0 - N_{dep}(t^+)}{L^+W^+z_{dep}^+} \ , \tag{10}$$

where $N_{dep}(t^+)$ is the number of particles deposited at time t^+, $A_d^+ = L^+W^+$ is the area of deposition and $V^+ = L^+W^+z_{dep}^+$ is the corresponding occupied volume. Here, L^+ and W^+ represent the non-dimensional length and width of the channel, whereas $z_{dep}^+ = d_p^+$ is the distance from the wall at which we assume a particle deposits.

To reproduce the condition of perfectly absorbing wall imposed by Uijttewaal and Oliemans (1996), particles are labelled as deposited even if they are subsequently re-entrained in the core region of the channel. We identify the deposition surface precisely at z_{dep}^+ to separate the core region of the channel from the deposition region. In this region, J^+ and C^+ are obtained from Eqs. 9 and 10 by counting the number of particles ΔN_{dep} deposited during subsequent time intervals Δt^+ (equal to 2.25 viscous time units in this study). Upon substitution of Eqs. 9 and 10 into Eq. 8, we obtain the following expression for the deposition coefficient:

$$k_d^+ = -\frac{\Delta N_{dep}(t^+)\ d_p^+}{\Delta t^+[N_0 - N_{dep}(t^+)]} \ . \tag{11}$$

Table 2 reports the non-dimensional values of the deposition coefficient, k_d^+, as function of particle Stokes number. For the range of Stokes numbers considered, sampling intervals of 450 wall time units (from $t^+ = 742$ to $t^+ = 1192$) were sufficient for obtaining converged deposition velocities, i.e. increases in the sampling interval did not appreciably change the deposition rate. The same values are also shown in the bi-logarithmic plot of Fig. 10 to visualize the trend. For comparison purposes, in Fig. 10 we also include the experimental

results already shown in Fig. 1 together with two empirical correlations between deposition coefficient and particle response time proposed by Liu & Agarwal (1974) - $k_d^+ = 6.00 \cdot 10^{-4} St^2$, boldface solid line - and by McCoy & Hanratty (1977) - $k_d^+ = 3.25 \cdot 10^{-4} St^2$, boldface dashed line. Both correlations show that, when scaled in wall units, the deposition rate can be correlated with the square of the response time for Stokes numbers varying from about 0.2 to 23. However, the large spread in experimental data on which the correlations are based indicates an uncertainty in the constant of proportionality, which can be estimated to be roughly 50% (van Haarlem et al., 1998). Uncertainty in estimates of the deposition rate is expected to affect also numerical data, particularly in the case of particles with small inertia: as St decreases, there are fewer depositing particles and it is difficult to obtain accurate values of the deposition rates. It is further difficult to estimate accurately the uncertainty of calculation of the deposition rate since the number of simulations required to obtained precise ensemble averages is quite expensive. As a consequence, there is little quantitative agreement among authors on the accurate value of deposition rates.

Results shown in Fig. 10 are qualitatively consistent with previous findings (Friedlander and Johnstone, 1957; Liu and Agarwal, 1974; Uijttewaal and Oliemans, 1996; Zhang and Ahmadi, 2000; Marchioli et al., 2003). A monotonic increase of the deposition coefficient with inertia is observed up to $St = 25$ for all flow configurations considered. For larger St, the deposition coefficient reaches a saturation level and becomes roughly independent of particle response time. It is clear from Fig. 10 that DNS calculations yield deposition rates which are in fair agreement with those obtained from the empirical correlations for $5 < St < 25$, while the deposition coefficient for the $St = 0.2$ and the $St = 1$ particles is much less than the experimental values. Overall, these values suggest that the deposition rate increases quadratically with particle response time whereas DNS predicts a dependence larger than St^2. This result is in agreement with those reported by Wang and Squires (1996) and by Wang et al. (1997).

Gravity does not modify the maximum value of deposition, which still occurs around $St = 25$ (Picciotto, et al., 2005b), yet it changes the quantitative value of k_d^+. For the smaller particles ($St = 0.2$), k_d^+ is increased by gravity in downflow and reduced in upflow. However,

these changes occur on very small values - $O(10^{-5} \div 10^{-6})$. For intermediate Stokes numbers ($1 < St < 15$), modifications due to gravity remain small and become important only for the larger Stokes numbers, which correspond to particles with large settling velocities. For these particles, maxima are smaller in downflow (case G_d, open squares) than in flow with no gravity (case G_0, open circles) and in upflow (case G_u, open triangles). As pointed out by Uijttewaal and Oliemans (1996), the reduced deposition coefficient in downward flow is likely due to the crossing trajectory effect, which makes the motion of large-inertia particles less correlated to the local turbulent flow field.

4. EFFECTS OF LIFT ON PARTICLE STATISTICS

In this Section the effects of lift on particle statistics are discussed. The lift force is expected to produce significant changes in particle behavior in turbulent shear flows (McLaughlin, 1991; Kurose and Komori, 1999). However, prediction of these changes is affected by the model used for the lift term in the equation of motion for the particles: results will differ depending on the model employed (Wang and Squires, 1996). In the present study, we used the model proposed by McLaughlin (1991) and later improved by Kurose & Komori (1999). Results are presented in the same fashion as done for Section 3: first, we will analyse the effect of lift on particle velocity statistics; then particle number density and particle deposition rates with and without lift will be compared for the different gravity set ups. Statistics were computed averaging over a time span of 450 wall units (which correspond to 3.6 non-dimensional response times of the larger particles considered in this study) starting from $t^+ = 742$.

4.1. Statistics of Particle Velocity

Fig. 11 shows the mean particle streamwise velocity, v_1^+, for each gravity set up and all particle time scales. As expected, profiles for the smaller particles ($St = 0.2$, Figs. 11a-c; and $St = 1$, Figs. 11d-f) are almost unaffected by the lift force. Modifications gradually appear as particle inertia increases, due to the larger velocity slip between particles and fluid

(see Fig. 5). This is particularly evident in the upflow/downflow configurations. Consider for instance the $St = 5$ particles: their streamwise velocity does not change when the lift force is applied in the no-gravity flow (Fig. 11g), yet the same velocity component starts to increase in the near-wall region ($z^+ < 10$) when lift and gravity act in tandem (Figs. 11h-i). A similar qualitative behavior is observed for the three larger particles, whose streamwise velocity profiles are weakly modified by lift in the simulations without gravity (Figs. 11l, 11o and 11r).

More evident modifications for these particles occur in vertical channel flow. In downflow, lift accelerates the $St = 15$ and the $St = 25$ particles everywhere except very close to the wall, in a thin fluid slab one wall unit thick where velocity profiles collapse onto each other (Figs. 11m and 11p, respectively). The reason for this behavior is not completely clear and deserves further investigation. In upflow (Figs. 11n and 11q), lift weakly slows the particles for $z^+ > 10$ and increases their streamwise velocity for $z^+ < 10$: in this near-wall fluid slab, v_1^+ remains positive even at the wall and particles are actually able to move upward. For the larger particles ($St = 125$), the velocity profile is not modified by lift in downflow (Fig. 11s); in contrast, applying lift in upflow (Fig. 11t) prevents the monotonic decrease of particle streamwise velocity near the wall producing an increase for $z^+ < 3$. This behavior can be explained considering the large velocity slip existing between particles of this size and the fluid: negative slip, due to particle velocity being lower than that of the fluid (as occurs in upflow), generates a repelling lift force directed away from the wall. On average, this repelling lift force prevents particles from reaching the wall unless they are entrained by strongly coherent in-sweeps (Marchioli and Soldati, 2002). Particles brought to the wall by in-sweeps end up in regions of higher-than-mean streamwise velocity. As particles adapt to the new fluid environment, they tend to sample preferentially high-speed near-wall regions (Kim et al., 1987).

Fig. 12 shows the particle wall-normal velocity, v_3^+. The velocity profiles shown in Figs. 12a-f are characterized by very small values around zero. The scatter in the data points, making the profiles a bit ragged, is likely due to the number of particles on which the calculation is based and to the time span chosen for averaging. Note that particles with small

inertia (the $St = 0.2$ particles in particular) are characterized by small mean values of v_3^+; the instantaneous values of v_3^+, however, scale with the wall-normal velocity fluctuations and can be orders of magnitude larger than the mean. We also remind that all statistics presented in this paper are relative to a statistically-developing condition for particle concentration: thus, the behavior of the wall-normal particle velocity just described is strongly dependent on the time interval over which profiles are computed. In the present study, profiles were computed from $t^+ = 742$ to $t^+ = 1192$. This early time interval allowed us to evaluate the evolution of the particle wall-normal velocity far from the condition of statistically-steady particle concentration, when profiles necessarily tend toward a zero value whatever the particle inertia.

In the no-gravity flow, lift appears to increase the drift of particles to the wall up to $St = 5$, yet producing small modifications on the profiles for both the $St = 0.2$ particles (Fig. 12a) and the $St = 1$ particles (Fig. 12d). For larger particle timescales and particularly for $St = 25$ (Fig. 12o), the effect is opposite and leads to a significant reduction of v_3^+. When also gravity is applied in either downflow or upflow, the presence of the velocity slip in the streamwise direction together with the lift force produces both quantitative and qualitative changes. For the downflow case, characterized by positive slip, these changes lead to an increase of particle drift velocity toward the wall, as profiles all shift toward the negative values (Figs. 12b to 12s along the central column). Completely different results are obtained for the upflow case (Figs. 12c to 12t along the right-hand column), in which lift acts to push particles away from the wall. It is apparent that lift reduces the average wall-normal velocity to very small values (close to zero) throughout the channel height. This occurs for all particles timescales with the exception of $St = 125$ (Fig. 12t). In this latter case, the shape of the velocity profile is maintained from a qualitative viewpoint: a quantitative reduction of the drift velocity still occurs, particularly in the range $20 < z^+ < 60$, but it is less dramatic.

The lift force is expected to modify the turbulent velocity fluctuations of the dispersed phase, as well. For sake of brevity, we do not show the statistics here (raw data are available on-line for interested readers): we only mention that significant quantitative modifications

are observed in the range $5 < St < 25$ at the "top" of the deposition curve, where the lift force is felt most strongly.

4.2. Particle Number Density Profiles

The effect of the lift force on particle number density, n_p, is shown in Fig. 13. In the absence of gravity, lift tends to increase the peak of particle number density at the wall up to $St = 5$ (Figs. 13a, 13d and 13g); a result which is in agreement with the increase in the wall-normal velocity observed in Fig. 12 for the same range of particle timescales. Also in agreement with the results of Fig. 12 is the reduced accumulation for the larger particles. Specifically, for the $St = 15$ particles (Fig. 13l) and for the $St = 25$ particles (Fig. 13o), this reduction occurs within 5 wall units from the wall, where a cross-over point is located. For larger distances from the wall, particle number density becomes larger when lift is applied. Profiles look qualitatively similar for the $St = 125$ particles (Fig. 13r), yet with smaller quantitative modifications. As for the statistics of particle velocity, the most interesting changes are observed for the two vertical flow configurations. First, lift tends to "pack" particles in downflow right at the wall (the last point in each profile), where a huge increase of particle number density is generated: this increase is roughly $O(10^2)$ for the $St = 1$ particles (Fig. 13e) and for the $St = 5$ particles (Fig. 13h); it is $O(10)$ for $St > 15$ (Figs. 13m, 13p and 13s, respectively). Second, the negative velocity slip occurring in upflow induces a repelling lift that acts to reduce wall accumulation (Figs. 13c to 13t in the right-hand column): in particular, this reduction leads to thin near-wall regions completely depleted of particles for the two smaller timescales (see Figs. 13c and 13f, where the value of n_p at the last point in the plot drops to zero). The lift force also appears to shift the number density peak toward the center of the channel. Consider the three larger particle sets, for instance: gravity alone generates a peak right at the wall, which moves at $z^+ \simeq 5$ when lift is applied (Figs. 13n, 13q and 13t).

The particle number density distributions for the cases without lift are produced by the occurrence of particle fluxes toward and away from the wall (Marchioli and Soldati, 2002)

which, in turn, are governed by different deposition mechanisms. These mechanisms are summarized in the schematic of Fig. 14a (Narayanan et al., 2003; Portela et al., 2002), where the log-law profile for the fluid velocity is also shown: (1) turbophoresis, a manifestation of the skewness in the velocity distribution of the particles (Reeks, 1983) which explains the tendency of the particles to drift from the bulk flow toward the near-wall accumulation region; (2) impaction deposition, representing the fraction of the turbophoretic drift which coasts through the accumulation region and deposits directly; and (3) 'diffusion' deposition, which removes particles from the accumulation region due to the residual turbulent fluctuations at the accumulation region. A fourth mechanism is due to turbulent diffusion, which acts to smooth the concentration gradients in the accumulation region. When the lift force is acting on the particles, it increases the turbophoretic drift in the downflow case (Fig. 14b) by increasing the particle wall-normal velocity (see Fig. 12, diagrams in the central column) so that particle deposition by impaction is favoured. On the contrary, the effect of lift in upflow (Fig. 14c) reduces the particle wall-normal drift velocity (see Fig. 12, diagrams in the right-hand column) and acts like an *additional* turbulent diffusion which removes particles away from the near-wall region. Note that, for visualization purposes, the particle number density profiles used in the sketches of Fig. 14b and Fig. 14c are those relative to the $St = 5$ particles.

4.3. Particle Deposition Rates

Table 3 reports the non-dimensional values of the deposition coefficient, k_d^+, for all flow configurations as function of particle Stokes number, St. The same values are also shown in the bi-logarithmic plot of Fig. 15 to visualize the trend. When particles are not subject to gravity (Fig. 15a), lift reduces the deposition coefficient for $St = 0.2$ and increases it for the intermediate timescales, particularly for $St = 5$. When particles are subject to gravity the deposition velocity may either increase or decrease depending on the direction of the shear-induced lift force. If gravity is in the flow direction (i.e. downflow, Fig. 15b), lift is toward the wall since the heavy particles lead the fluid. Therefore, the deposition rate

increases. If gravity is in the opposite direction (i.e. upflow, Fig. 15c), the lift force tends to move the particles away from the wall and the deposition rate decreases. From a qualitative viewpoint, similar variations of the deposition velocity were observed by Zhang and Ahmadi (2000) for heavy particles ($\rho_p/\rho_f = 10^3$ and $2 \cdot 10^3$) with Stokes numbers up to $St = 10$ in vertical channel flow at $Re_\tau = 125$. However, these authors computed the deposition velocity during the first 100 time wall units of the simulation using samples of 8192 particles per Stokes number. These differences make the quantitative comparison very difficult.

In downflow (Fig. 15b), lift enhances particle deposition rate up to $St = 25$: in particular, k_d^+ increases by roughly two orders of magnitude in the range $0.2 \leq St \leq 5$. In upflow (Fig. 15c), a reduction for $0.2 \leq St \leq 1$ and an increase for $St = 5$ is observed. Whichever is the flow configuration, however, the qualitative behavior of the particle deposition rate does not undergo a radical modification because of the lift force. As shown in Fig. 15, the trend of each deposition curve with respect to the particle Stokes number is maintained, this being particularly true for the larger particles ($St = 125$). Although leading the fluid in the near-wall region, the motion of these particles is not much affected while travelling across the relatively thin near-wall layer (Uijttewaal and Oliemans, 1996).

In our opinion, the results just discussed provide useful information to develop engineering models for prediction of deposition rates and concentration distribution in wall-bounded flows. Recalling the deposition mechanisms illustrated in Fig. 14, the time derivative of particle concentration in the accumulation region can be expressed by the following volume flux balance equation:

$$\frac{\mathrm{d}C}{\mathrm{d}t} = \Phi^{in} - \Phi^{out} = \Delta\Phi \geq 0 \ , \tag{12}$$

where Φ^{in} is the total volume flux of particles entering the accumulation region either from the core region of the flow (due to turbophoresis) or from the wall (due to turbulent diffusion) and Φ^{out} is the total volume flux of particles exiting the accumulation region either toward the core region of the flow (due to re-entrainment by ejection events) or toward the wall (due to diffusional deposition). Clearly, the condition $\mathrm{d}C/\mathrm{d}t = \Delta\Phi = 0$ holds at steady state.

According to Eq. 11, one can write:

$$\Delta\Phi = \frac{\mathrm{d}J}{\mathrm{d}z} = k_d \frac{\mathrm{d}C}{\mathrm{d}z} \ , \tag{13}$$

and the deposition coefficient, k_d, must be computed considering the different deposition mechanisms by which it is modified. For particles in the diffusion-impaction regime, in particular, diffusion deposition and impaction deposition appear the most important competing mechanisms (Marchioli et al., 2003; Narayanan et al. 2003). From a practical engineering viewpoint, it is of importance to develop deposition models capable of accounting for both mechanisms. A rather simple model of this kind has been developed by Soldati and Andreussi (1996) basing on the assumption of diffusion and impaction acting in parallel. Thus, the total deposition coefficient is given by:

$$k_d = V_I k_I + (1 - V_I) k_D \ , \tag{14}$$

where V_I represents the volume fraction of particles depositing by impaction, k_I is the impaction deposition coefficient and k_D is the diffusion deposition coefficient. The present DNS database could be used to evaluate the quantities on the right-hand side of Eq. 14 and to estimate the quantitative modifications they undergo due to lift.

5. CONCLUSIONS

In this paper, we address the problem of quantifying the effects of gravity and lift on particle dispersion and deposition in wall-bounded turbulent flows. To this aim, detailed statistics of particle velocity and deposition rates were obtained from direct numerical simulation of fully-developed channel flow at low Reynolds number. Different flow configurations (flow with no gravity, vertical downflow and vertical upflow) and several values of the particle Stokes number, namely the particle timescale, were considered to cover a broad range of situations. The data resulting from this study apply to dilute dispersed systems and can hardly be obtained by experiments. They are made available as ASCII files at HTTP://CFD.CINECA.IT (mirror site: HTTP://158.110.32.35/DOWNLOAD/DATABASE) for possible use in validation of engineering models for particle dispersion.

Results put forth in this paper show first the influence of gravity on particle wall accumulation and on particle deposition rate via the crossing-trajectory effect. In particular, it is observed that quantitative modifications on the statistics become relevant starting from particles with $St \simeq 25$, a value which can be roughly viewed as threshold to discriminate between "small" and "large" particles. In the case of small particles, gravity has little effect on their average settling velocity, which tends to remain smaller than the average turbulent fluctuating velocities. More generally, the impact of gravity on the motion of these small particles is rather weak and leads to negligible quantitative modifications of the statistics. In the case of large particles, velocity correlations along the particle trajectories tend to decrease due to the crossing-trajectory effect and particle motion becomes disengaged from fluid turbulence. This leads to quantitative changes in the accumulation process, which also depend on the gravity setup being considered, and to modified statistics of particle velocity. Results obtained for the deposition coefficient are fully representative of this behavior.

The present datasets also include particle velocity and deposition statistics that quantify the effect of the lift force on particles. Neglecting this effect can become very stringent since the lift force can modify particle accumulation rates under given conditions (Uijttewaal and Oliemans, 1996; Marchioli et al., 2003). For instance, it can reduce wall accumulation in an upward pipe flow for particle timescales in the range $3.8 < St < 27.9$ (Marchioli et al., 2003). The accuracy of the model used to reproduce the effect of the lift force in the particle equation of motion is also important. In the present study, a model accounting for linear shear flow conditions and high particle Reynolds numbers is used, which is more appropriate for simulations of wall-bounded turbulent shear flows than the Saffman formula.

Present results demonstrate that lift may have a significant effect on the mean particle drift velocity toward the wall (which is modified throughout the channel height) and, in turn, on particle accumulation in the near-wall region. This effect becomes more and more evident as the particle timescale is increased and is observed in each flow configuration. Evaluation of the deposition rate indicates that changes due to lift will be quantitatively different depending on the particle timescale. Specifically, the rate at which particles with $St > 25$ deposit is almost unaffected by lift whereas smaller particles will either increase or

decrease their deposition rate depending on the orientation on gravity with respect to the mean flow.

The accumulation of particles in the near-wall region indicates that gravity and lift modify the statistics of the dispersed phase mostly from a quantitative viewpoint, in agreement with the conclusion that the non-homogeneity of particle distribution is primarily a result of the dynamic interaction occuring between particles and near-wall turbulent structures. In this respect, all other forces acting on particles appear to simply superpose and, eventually, merge their effects. As the non-homogeneity of particle distribution builds up over time, regions in which the dilute system assumption locally breaks down may appear. The present results would be of limited value in these regions. However, because of the relatively small volume fraction occupied by the particles, their effect on turbulence is expected to be rather small in the time span within which statistics were computed.

ACKNOWLEDGMENTS

Financial support from MAP-ICE-CRUI under Grant *Sviluppo di sistemi innovativi per la pre-separazione di nano/micro particelle da flussi di processo* is gratefully acknowledged.

REFERENCES

1. Brooke, J.W., Hanratty, T.J., McLaughlin, J.B., 1994. Free-flight mixing and deposition of aerosols. Phys. Fluids A, 6, 3404-3414.

2. Cousins, L.B., Hewitt, G.F., 1968. Liquid phase mass transfer in annular two-phase flow. UKAEA Report, AERE-R 5657, 1968.

3. Csanady, G.T., 1963. Turbulent diffusion of heavy particles in the atmosphere. J. Atmos. Sci., 20, 201-208.

4. Elghobashi, S., Abou-Arab, T.W., 1983. A two-equation turbulence model for two-phase flows. Phys. Fluids, 26(4), 931-938.

5. Elghobashi, S., Truesdell, G.C., 1992. Direct simulation of particle dispersion in a decaying isotropic turbulence. J. Fluid Mech., 242, 655-700.

6. Friedlander, S.K., Johnstone, H.F., 1957. Deposition of suspended particles from turbulent gas streams. Ind. Eng. Chem. Res., 49, 1151-1156.

7. Giusti, A., Lucci, F., Soldati, A., 2005. Influence of the lift force in direct numerical simulation of upward/downward turbulent channel flow laden with surfactant contaminated microbubbles. Chem. Eng. Sci., 60, 6176-6187.

8. van Haarlem, B., Boersma, B.J., Nieuwstadt, F.T.M., 1998. Direct numerical simulation of particle deposition onto a free-slip and no-slip surface, Phys. Fluids A, 10, 2608-2620.

9. Kaftori, D., Hetsroni, G., Banerjee, S., 1995a. Particle behavior in the turbulent boundary layer. I. Motion, deposition and entrainment. Phys. Fluids A, 7, 1095-1106.

10. Kaftori, D., Hetsroni, G., Banerjee, S., 1995b. Particle behavior in the turbulent boundary layer. II. Velocity and distribution profiles. Phys. Fluids A, 7, 1107-1121.

11. Kim, J., Moin, P., Moser, R., 1987. Turbulence statistics in fully developed channel flow at low Reynolds number. J. Fluid Mech., 177, 133-166.

12. Kurose, R., Komori, S., 1999. Drag and lift forces on a rotating sphere in a linear shear flow. J. Fluid Mech., 103, 183-206.

13. Lam, K., Banerjee, S., 1992. On the condition of streak formation in bounded flows. Phys. Fluids A, 4, 306-320.

14. Liu, B.Y., Agarwal, J.K., 1974. Experimental observation of aerosol deposition in turbulent flow. J. Aerosol Sci., 5, 145-148.

15. Lyons, S.L., Hanratty, T.J., McLaughlin, J.B., 1991. Large-scale computer simulation of fully developed turbulent channel flow with heat transfer. Int. J. Num. Meth. Fluids, 13, 999-1028.

16. Marchioli, C., Soldati, A., 2002. Mechanisms for particle transfer and segregation in turbulent boundary layer. J. Fluid Mech., 468, 283-315.

17. Marchioli, C., Giusti, A., Salvetti, M.V., Soldati, A., 2003. Direct numerical simulation of particle wall transfer and deposition in upward turbulent pipe flow. Int. J. Multiphase Flow, 29, 1017-1038.

18. Maxey, M.R., Riley, J.K., 1983. Equation of motion for a small rigid sphere in a nonuniform flow. Phys. Fluids A, 26, 883-889.

19. Maxey, M.R., 1987. The gravitational settling of aerosol particles in homogeneous turbulence and random flow fields. J. Fluid Mech., 174, 441-465.

20. McCoy, D.D., Hanratty, T.J., 1977. Rate of deposition of droplets in annular two-phase flow. Int. J. Multiphase Flow, 3, 319-331, 1977.

21. McLaughlin, J.B., 1989. Aerosol particle deposition in numerically simulated channel flow. Phys. Fluids A, 1, 1211-1224.

22. McLaughlin, J.B., 1991. Inertial migration of a small sphere in linear shear flows. J. Fluid Mech., 224, 261-274.

23. Narayanan, C., Lakehal, D., Botto, L., Soldati, A., 2003. Mechanisms of particle deposition in a fully developed turbulent channel flow. Phys. Fluids, 15, 763-775.

24. Niño, N., Garcia, M.H., 1996. Experiments on particle-turbulence interactions in the near-wall region of an open channel flow: implications for sediment transport. J. Fluid Mech., 326, 285-319.

25. Pan, Y., Banerjee, S., 1996. Numerical simulation of particle interactions with wall turbulence. Phys. Fluids A, 8, 2733-2755.

26. Picciotto, M., Marchioli, C., Reeks, M.W., Soldati, A., 2005a. Statistics of velocity and preferential accumulation of micro-particles in boundary layer turbulence. Nucl. Eng. Des., 235, 1239-1249.

27. Picciotto, M., Marchioli, C., Soldati, A., 2005b. Characterization of near-wall accumulation regions for inertial particles in turbulent boundary layers. Phys. Fluids, 17, 098101.

28. Portela, L.M., Cota, P., Oliemans, R.V.A., 2002. Numerical study of the near-wall behaviour of particles in turbulent pipe flows. Powd. Tech., 125, 149-157.

29. Reeks, M.W., 1983. The transport of discrete particles in inhomogeneous turbulence. J. Aerosol Sci., 310, 729-739.

30. Righetti, M., Romano, G.P., 2004. Particle-fluid interactions in a plane near-wall turbulent flow. J. Fluid Mech., 505, 93-121.

31. Rouson, D.W.I., Eaton, J.K., 2001. On the preferential concentration of solid particles in channel flow. J. Fluid Mech., 428, 149-169.

32. Saffman, P.G., 1965. The lift on a small sphere in a slow shear flow. J. Fluid Mech. 22, 385-400, and Corrigendum 31, 624 (1968).

33. Sergeev, Y.A., Johnson, R.S., Swailes, D.C., 2002. Dilute suspension of high inertia particles in the turbulent flow near the wall. Phys. Fluids A, 14, 1042-1055.

34. Soldati, A., 2003. Cost/efficiency analysis of a wire-plate ESP with an advection diffusion equation for turbulent particle transport. Aerosol Sci. Technol., 37, 171-182.

35. Soldati, A., 2005. Particles turbulence interactions in boundary layers. ZAMM - J. of Applied Mathematics and Mechanics, 85, 683-699.

36. Soldati, A., Andreussi, P., 1996. The influence of coalescence on droplet transfer in vertical annular flow. Chem. Engng. Sci., 51, 353-363.

37. Soltani, M., Ahmadi, G., 1995. Direct numerical simulation of particle entrainment in turbulent channel flow. Phys. Fluids A, 7, 647-657.

38. Uijttewaal, W.S., Oliemans, R.V.A., 1996. Particle dispersion and deposition in direct numerical and large eddy simulations of vertical pipe flows. Phys. Fluids A, 8, 2590-2604.

39. Wang, Q., Squires, K.D., 1996. Large eddy simulation of particle deposition in a vertical turbulent channel flow. Int. J. Multiphase Flow, 22, 667-683.

40. Wang, Q., Squires, K.D., Chen, M., McLaughlin, J.B., 1997. On the role of the lift force in turbulence simulations of particle deposition. Int. J. Multiphase Flow, 23, 749-763.

41. Wells, M.R., Stock, D.E., 1983. The effect of crossing trajectories on the dispersion of particles in a turbulent flow. J. Fluid Mech., 136, 31-62.

42. Young, J.B., Leeming, A., 1997. A theory of particle deposition in turbulent pipe flow. J. Fluid Mech., 340, 129-159.

43. Zhang, H., Ahmadi, G., 2000. Aerosol particle transport and deposition in vertical and horizontal turbulent duct flows. J. Fluid Mech., 406, 55-80.

TABLE CAPTIONS

Table 1 : Parameters relevant to the simulations of particle dispersion. Superscript + identifies non-dimensional variables. Note that, in the present study, $St = \tau_p^+ = \tau_p/\tau_f$ by definition.

Table 2 : Deposition coefficient, k_d^+, as function of particle Stokes number, St (simulations without lift). Statistics are time averaged from $t^+ = 742$ to $t^+ = 1192$.

Table 3 : Deposition coefficient, k_d^+, as function of particle Stokes number, St, for simulations with lift. Statistics are time averaged from $t^+ = 742$ to $t^+ = 1192$.

FIGURE CAPTIONS

Figure 1 : Particle deposition from fully-developed turbulent pipe flow: a summary of experimental data (courtesy of Young and Leeming, 1997).

Figure 2 : Flow configurations: no-gravity flow (G_0), vertical downflow (G_d, gravity directed along the positive x-axis) and vertical upflow (G_u, gravity directed along the negative x-axis).

Figure 3 : Instantaneous particle number density, n_p, as a function of wall distance, z^+, at $t^+ = 675$ (left column) and at $t^+ = 1125$ (right column). (a-b) $St = 0.2$, (c-d) $St = 1$, (e-f) $St = 5$, (g-h) $St = 15$, (i-l) $St = 25$, (m-n) $St = 125$. Symbols: + no gravity; ■ downflow; ◯ upflow.

Figure 4 : Maximum value of particle number density at the wall, n_p^{max}, as function of time, t^+. (a) $St = 0.2$, (b) $St = 1$, (c) $St = 5$, (d) $St = 15$, (e) $St = 25$, (f) $St = 125$. Symbols: + no gravity; ■ downflow; ◯ upflow.

Figure 5 : Mean streamwise velocity, v_1^+, as a function of wall distance, z^+. Statistics are time averaged from $t^+ = 742$ to $t^+ = 1192$. (a) $St = 0.2$, (b) $St = 1$, (c) $St = 5$, (d) $St = 15$, (e) $St = 25$, (f) $St = 125$. Solid line: fluid. Symbols: + no gravity; ■ downflow; ◯ upflow.

Figure 6 : Mean wall-normal velocity, v_3^+, as a function of wall distance, z^+. Statistics are time averaged from $t^+ = 742$ to $t^+ = 1192$. (a) $St = 0.2$, (b) $St = 1$, (c) $St = 5$, (d) $St = 15$, (e) $St = 25$, (f) $St = 125$. Solid line: fluid. Symbols: + no gravity; ■ downflow; ◯ upflow.

Figure 7 : Root mean square of particle streamwise velocity, $v_1^{+,rms}$, as a function of wall distance, z^+. Statistics are time averaged from $t^+ = 742$ to $t^+ = 1192$. (a) $St = 0.2$, (b) $St = 1$, (c) $St = 5$, (d) $St = 15$, (e) $St = 25$, (f) $St = 125$. Dashed line: fluid. Symbols: + no gravity; ■ downflow; ◯ upflow.

Figure 8 : Root mean square of particle wall-normal velocity, $v_3^{+,rms}$, as a function of wall distance, z^+. Statistics are time averaged from $t^+ = 742$ to $t^+ = 1192$. (a) $St = 0.2$, (b) $St = 1$, (c) $St = 5$, (d) $St = 15$, (e) $St = 25$, (f) $St = 125$. Dashed line: fluid. Symbols: + no gravity; ■ downflow; ◯ upflow.

Figure 9 : Mean particle Reynolds number, Re_p, as a function of wall distance, z^+. (a) $St = 0.2$, (b) $St = 1$, (c) $St = 5$, (d) $St = 15$, (e) $St = 25$, (f) $St = 125$. Symbols: + no gravity; ■ downflow; ◯ upflow.

Figure 10 : Deposition coefficient, k_d^+, as function of particle Stokes number, St. Statistics are time averaged from $t^+ = 742$ to $t^+ = 1192$. Symbols: ◯ no gravity; □ downflow; △ upflow.

Figure 11 : Mean streamwise velocity, v_1^+, as a function of wall distance, z^+. Statistics are time averaged from $t^+ = 742$ to $t^+ = 1192$. (a-c) $St = 0.2$, (d-f) $St = 1$, (g-i) $St = 5$, (l-n) $St = 15$ (o-q) $St = 25$, (r-t) $St = 125$. Symbols: + no gravity, ▼ no gravity with lift; ■ downflow, ▽ downflow with lift; ◯ upflow, ▲ upflow with lift.

Figure 12 : Mean wall-normal velocity profiles, v_3^+, as a function of wall distance, z^+. Statistics are time averaged from $t^+ = 742$ to $t^+ = 1192$. (a-c) $St = 0.2$, (d-f) $St = 1$, (g-i) $St = 5$, (l-n) $St = 15$ (o-q) $St = 25$, (r-t) $St = 125$. Symbols: + no gravity, ▼ no gravity with lift; ■ downflow, ▽ downflow with lift; ◯ upflow, ▲ upflow with lift.

Figure 13 : Instantaneous particle number density profiles, n_p, as a function of wall distance, z^+. Statistics are calculated at $t^+ = 1125$. (a-c) $St = 0.2$, (d-f) $St = 1$, (g-i) $St = 5$, (l-n) $St = 15$ (o-q) $St = 25$, (r-t) $St = 125$. Symbols: + no gravity, ▼ no gravity with lift; ■ downflow, ▽ downflow with lift; ◯ upflow, ▲ upflow with lift.

Figure 14 : Near-wall driving mechanisms, responsible for particle concentration

build-up in the near-wall accumulation region (a) and effect of lift on particle concentration in the case of downflow (b) and in the case of upflow (c).

Figure 15 : Particle deposition coefficients, k_d^+, as a function of the Stokes number, St. Statistics are time averaged from $t^+ = 742$ to $t^+ = 1192$. No gravity (a); vertical downward (b); vertical upward (c). Symbols: + no gravity, ▼ no gravity and lift; ■ downflow, ▽ downflow and lift; ◯ upflow, ▲ upflow with lift.

$St = \tau_p^+$	$\tau_p\ (s)$	d_p^+	$d_p\ (\mu m)$	$V_s^+ = g^+ St$	$Re_p^+ = \frac{V_s^+ d_p^+}{\nu^+}$
0.2	$2.265 \cdot 10^{-4}$	0.068	9.12	0.019	$1.4 \cdot 10^{-3}$
1	$1.133 \cdot 10^{-3}$	0.153	20.4	0.094	0.014
5	$5.660 \cdot 10^{-3}$	0.342	45.6	0.472	0.161
15	$1.698 \cdot 10^{-2}$	0.586	78.2	1.416	0.829
25	$2.832 \cdot 10^{-2}$	0.765	102	2.360	1.805
125	$1.415 \cdot 10^{-1}$	1.71	228	11.79	20.158

Table 1 - “Influence of gravity and lift...” - Marchioli et al.

$St = \tau_p^+$	$k_d^+\|_{G_0}$	$k_d^+\|_{G_u}$	$k_d^+\|_{G_d}$
0.2	$0.333E-05$	$0.190E-05$	$0.666E-05$
1	$0.200E-04$	$0.167E-04$	$0.266E-04$
5	$0.349E-02$	$0.284E-02$	$0.276E-02$
15	$0.410E-01$	$0.380E-01$	$0.292E-01$
25	$0.799E-01$	$0.750E-01$	$0.415E-01$
125	$0.110E+00$	$0.701E-01$	$0.301E-01$

Table 2 - "Influence of gravity and lift..." - Marchioli et al.

$St = \tau_p^+$	$k_d^+\|_{G_0}$	$k_d^+\|_{G_u}$	$k_d^+\|_{G_d}$
0.2	$0.126E-05$	$0.000E+00$	$0.236E-03$
1	$0.300E-04$	$0.333E-05$	$0.680E-02$
5	$0.168E-01$	$0.614E-02$	$0.704E-01$
15	$0.968E-01$	$0.455E-01$	$0.747E-01$
25	$0.120E+00$	$0.761E-01$	$0.614E-01$
125	$0.122E+00$	$0.557E-01$	$0.314E-01$

Table 3 - "Influence of gravity and lift..." - Marchioli et al.

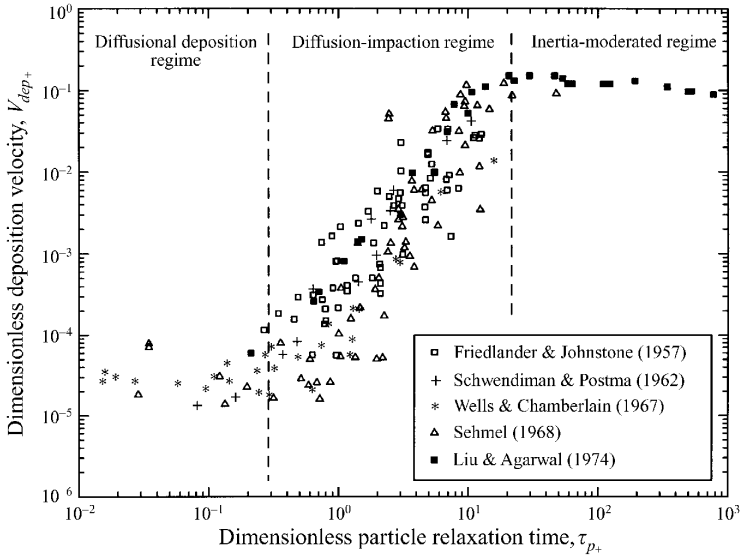

Figure 1 - "Influence of gravity and lift..." - Marchioli et al.

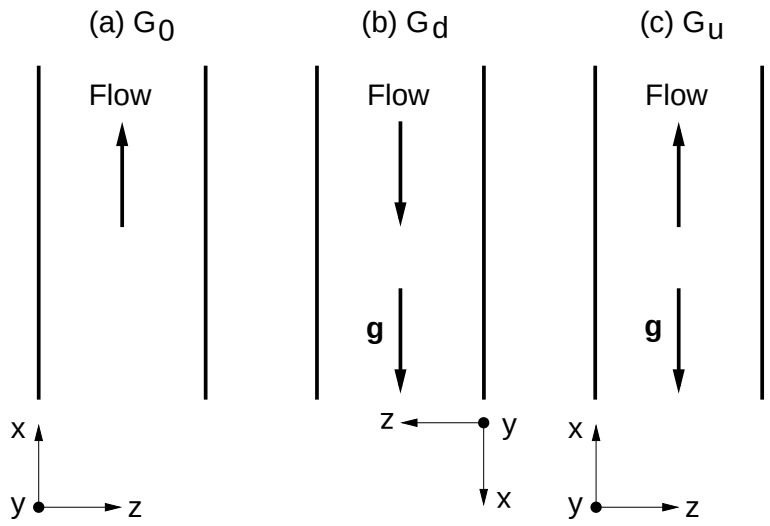

Figure 2 - "Influence of gravity and lift..." - Marchioli et al.

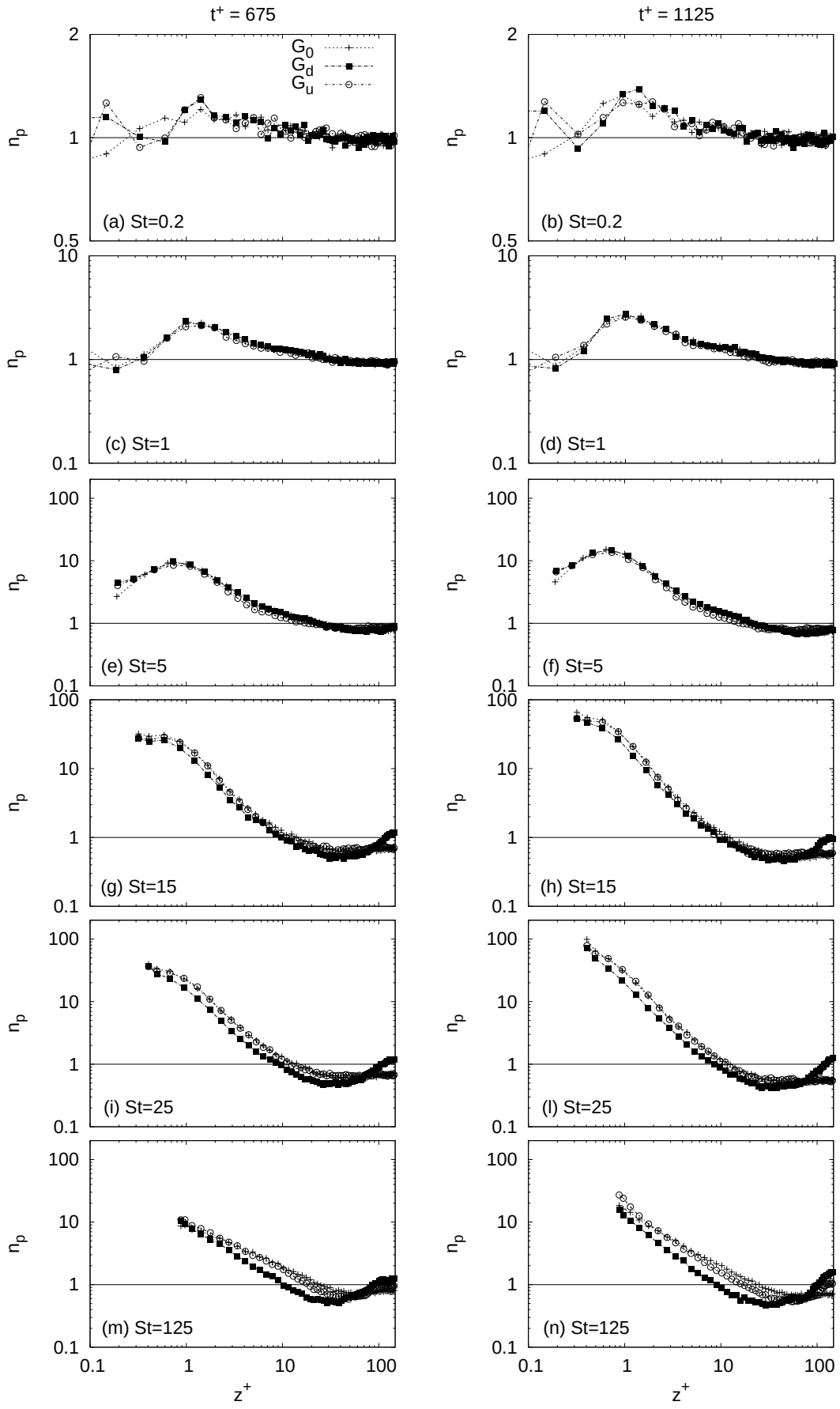

Figure 3 - "Influence of gravity and lift..." - Marchioli et al.

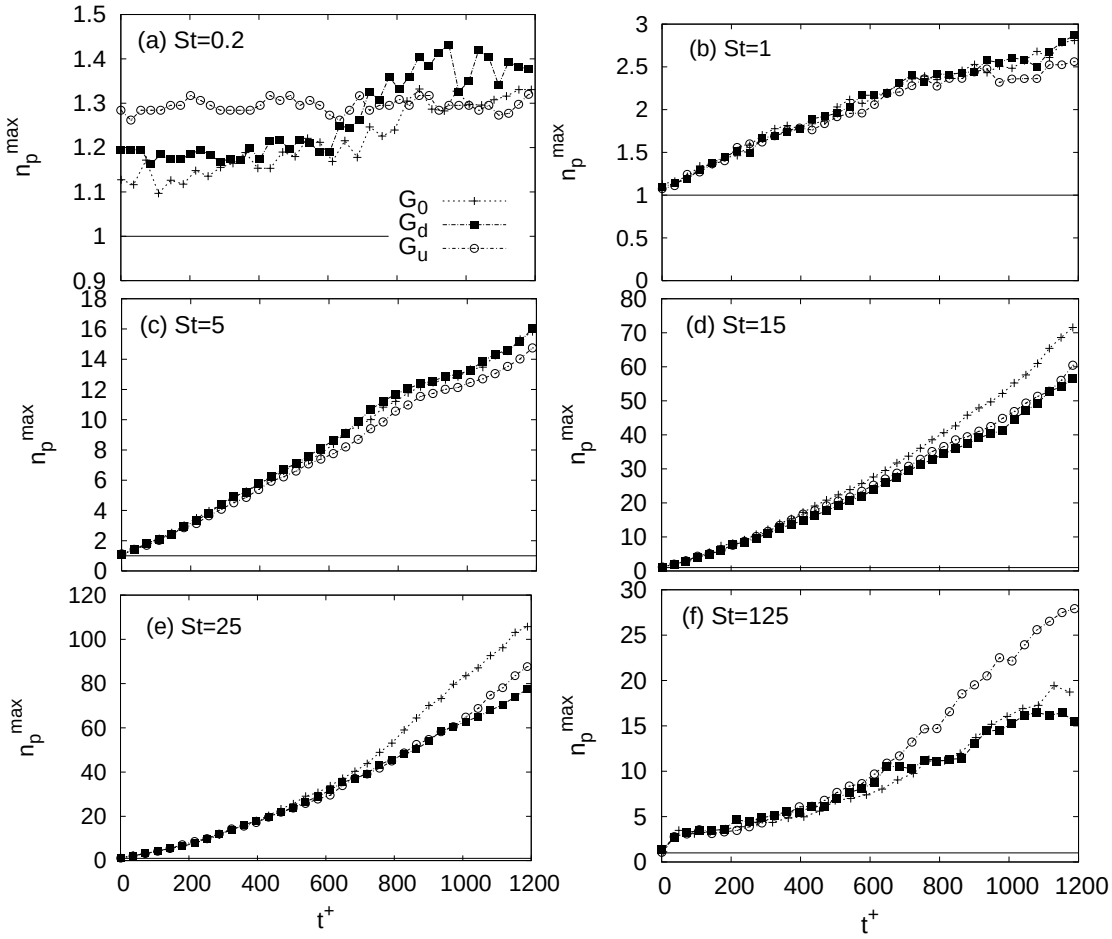

Figure 4 - "Influence of gravity and lift..." - Marchioli et al.

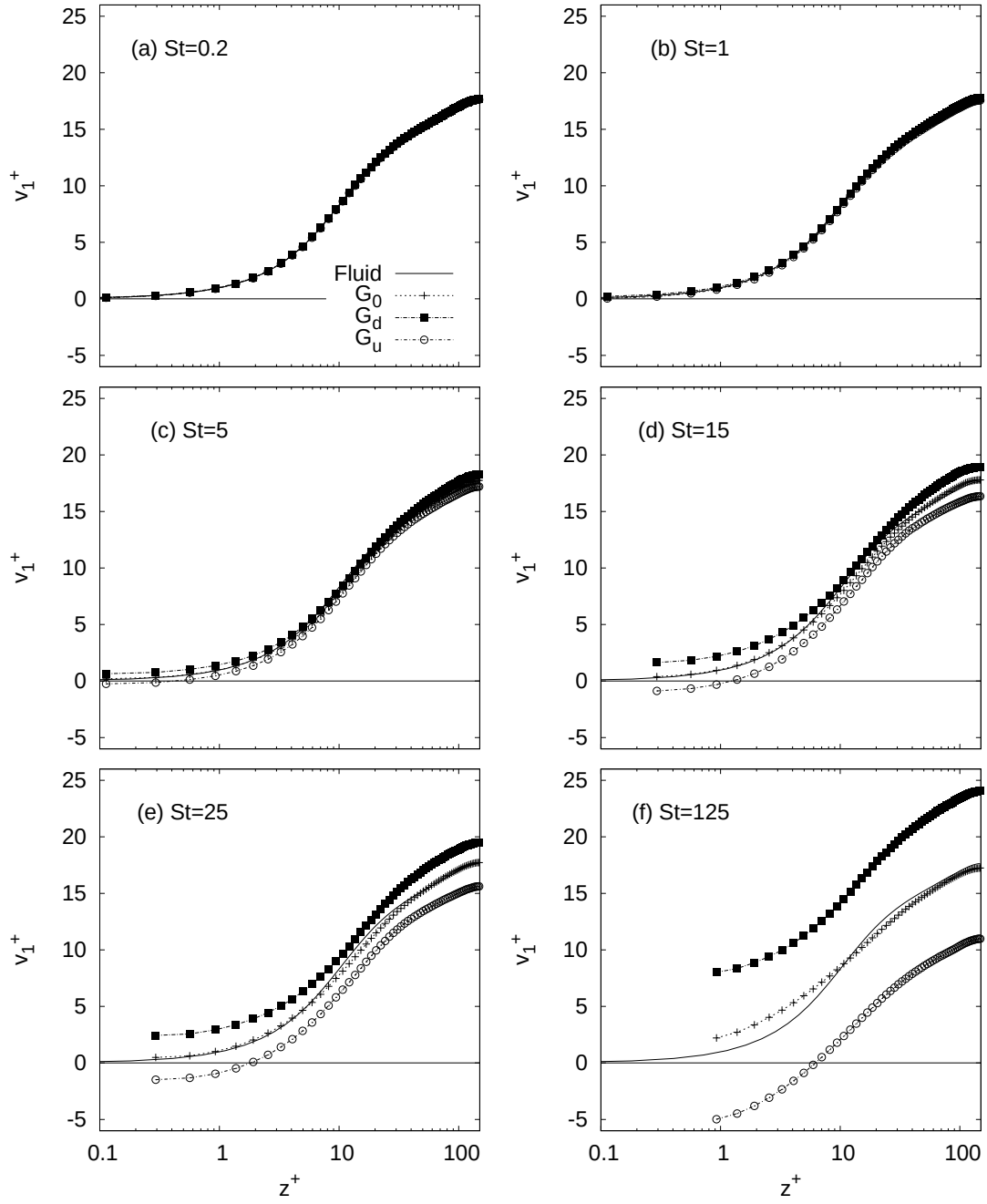

Figure 5 - "Influence of gravity and lift..." - Marchioli et al.

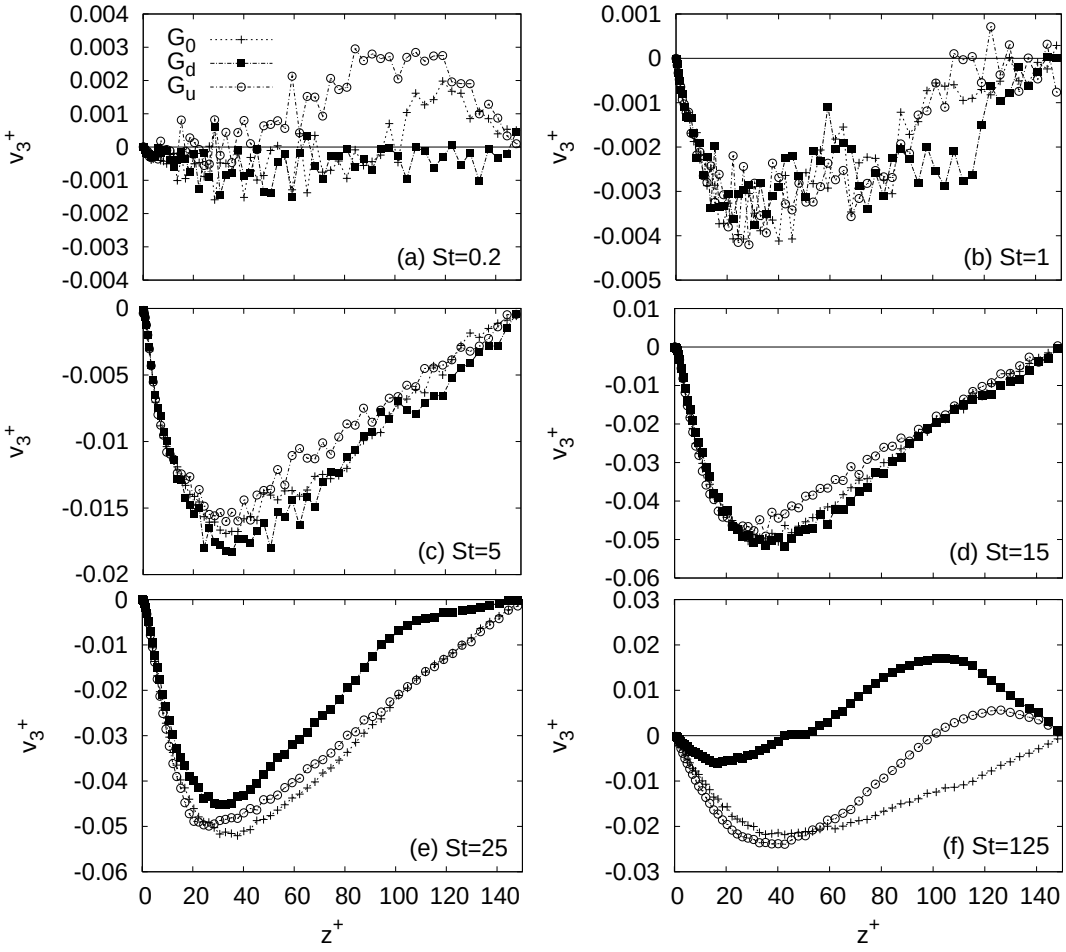

Figure 6 - "Influence of gravity and lift..." - Marchioli et al.

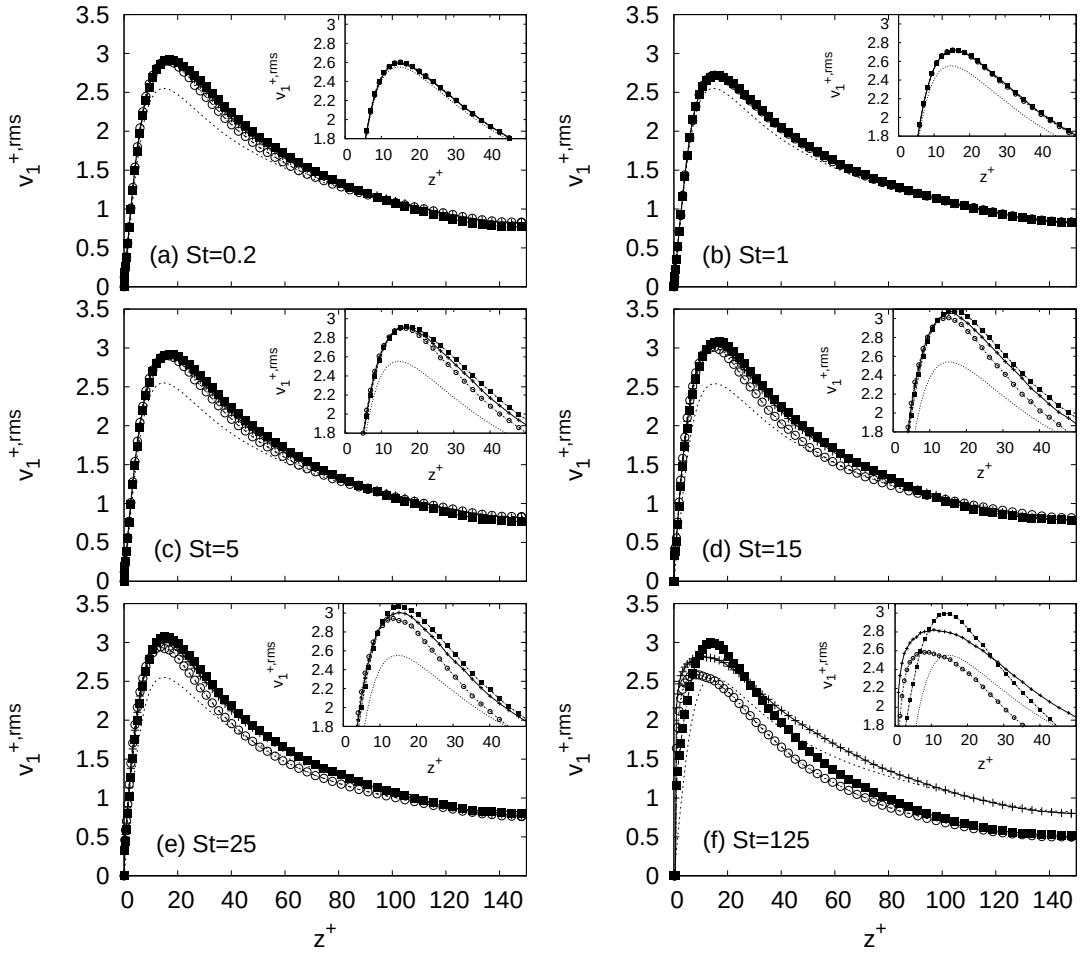

Figure 7 - "Influence of gravity and lift..." - Marchioli et al.

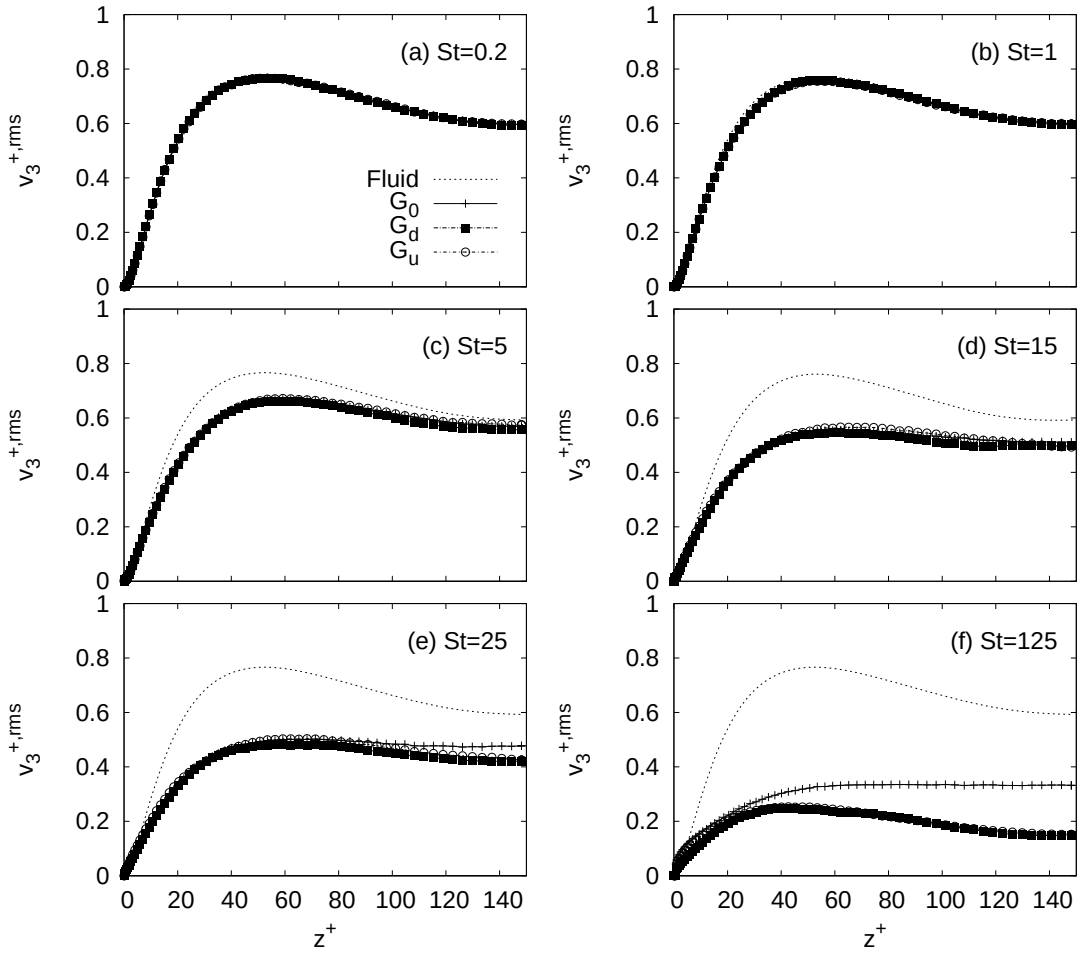

Figure 8 - "Influence of gravity and lift..." - Marchioli et al.

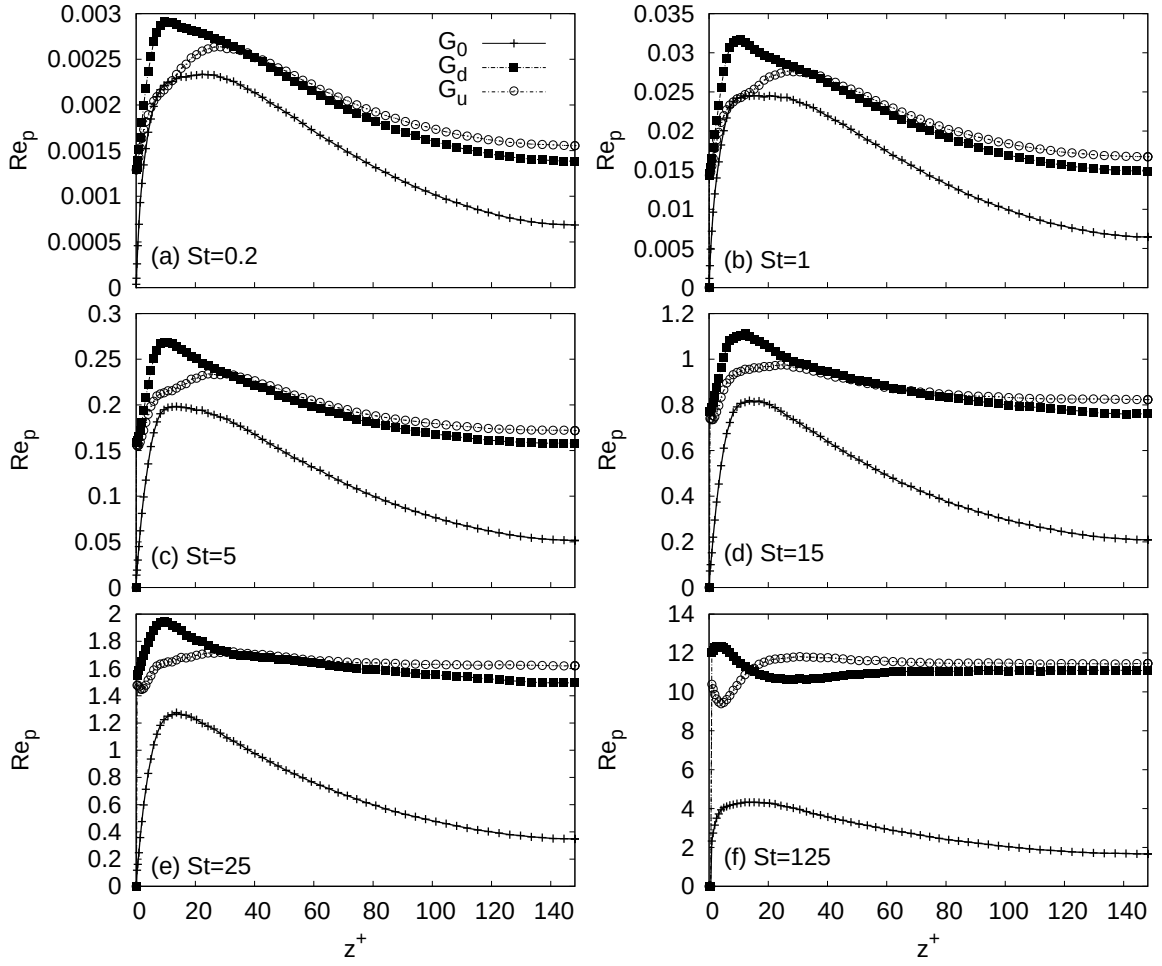

Figure 9 - "Influence of gravity and lift..." - Marchioli et al.

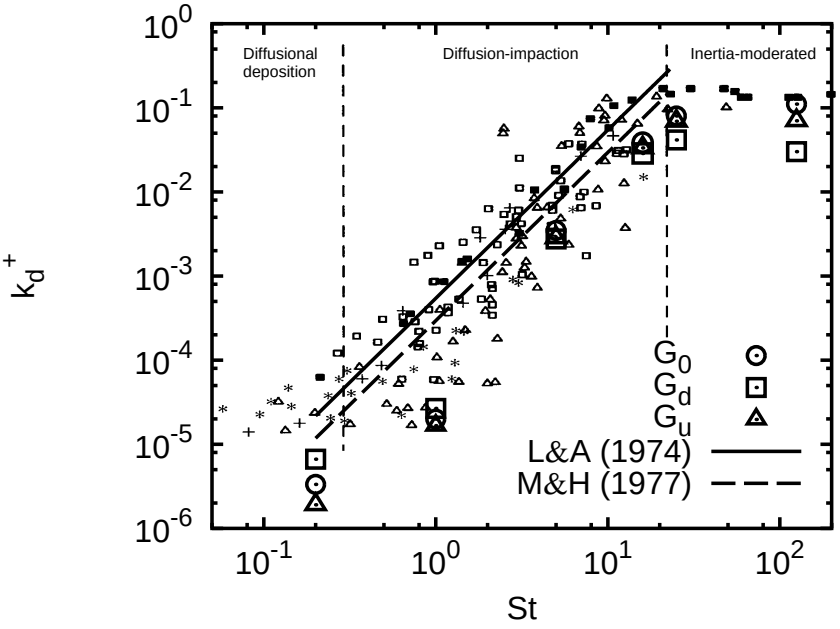

Figure 10 - "Influence of gravity and lift..." - Marchioli et al.

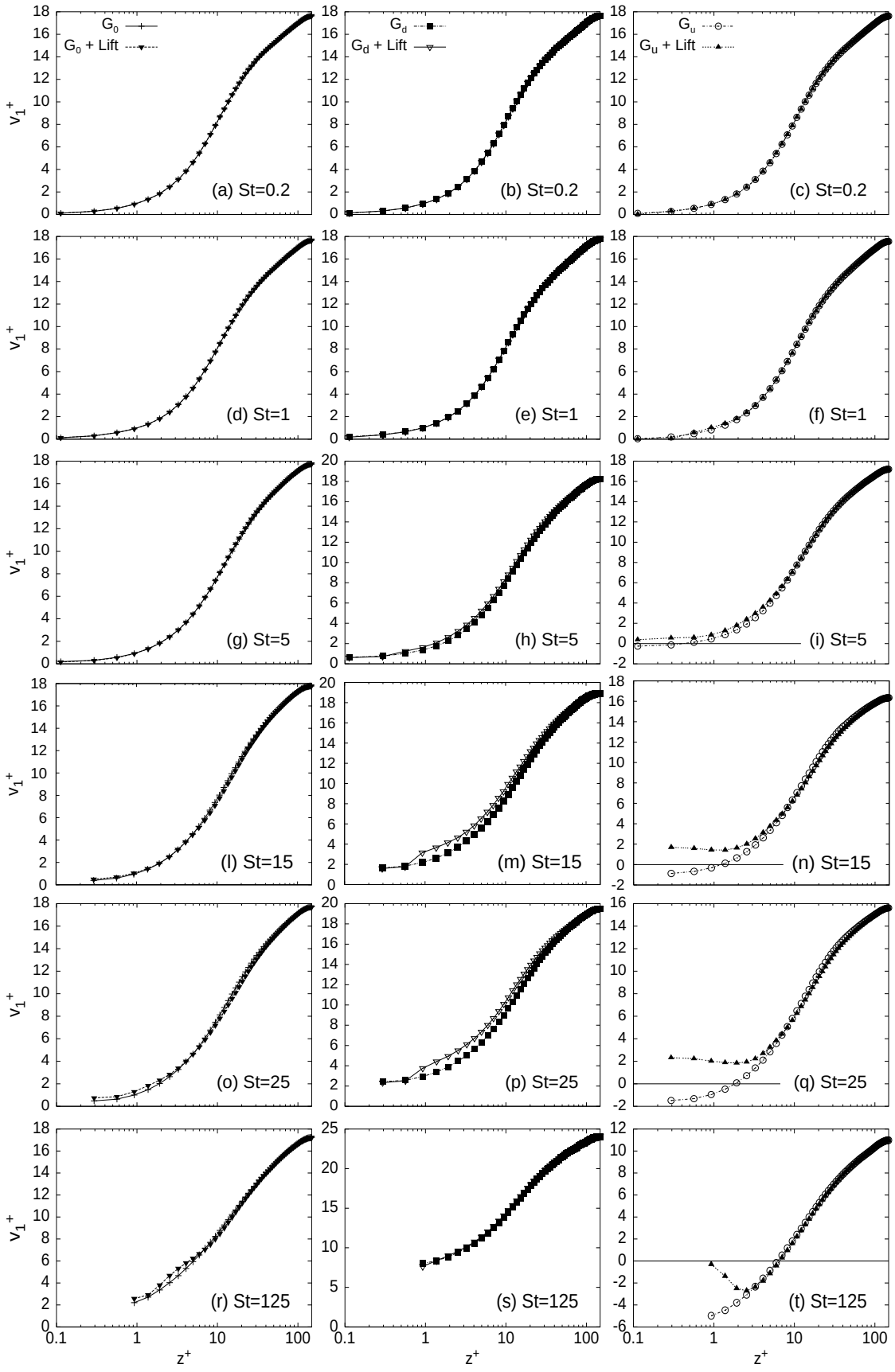

Figure 11 - "Influence of gravity and lift..." - Marchioli et al.

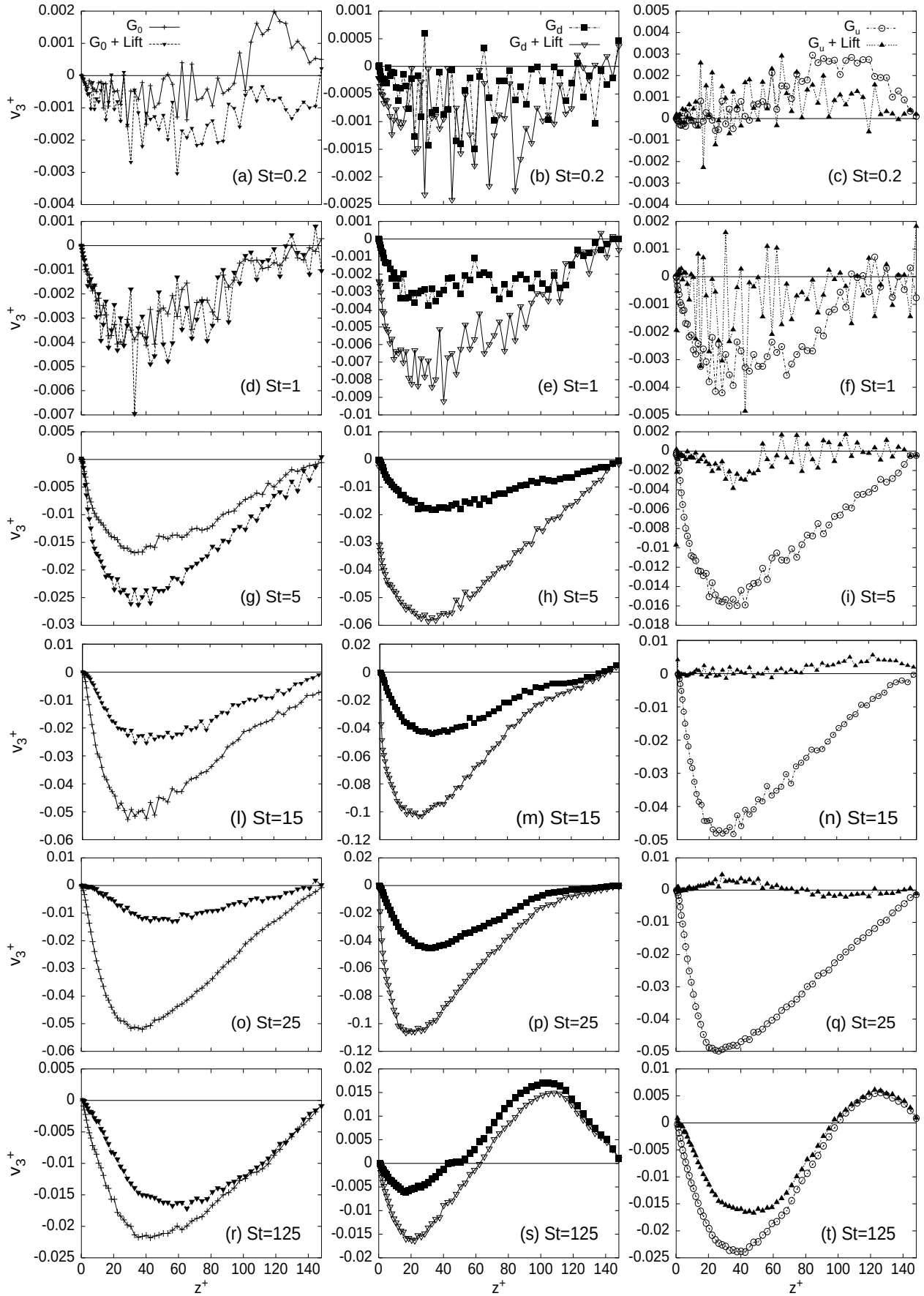

Figure 12 - "Influence of gravity and lift..." - Marchioli et al.

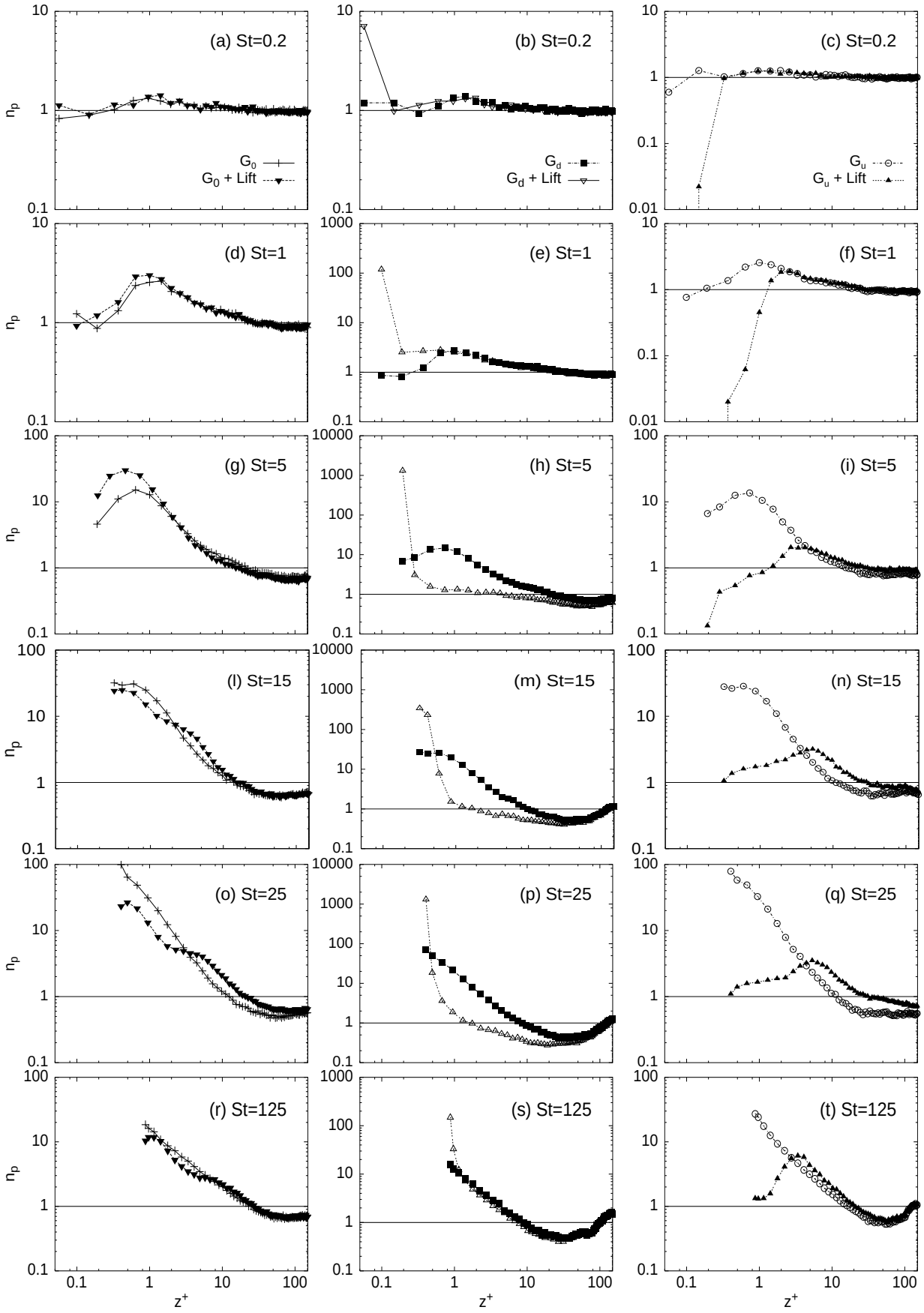

Figure 13 - "Influence of gravity and lift..." - Marchioli et al.

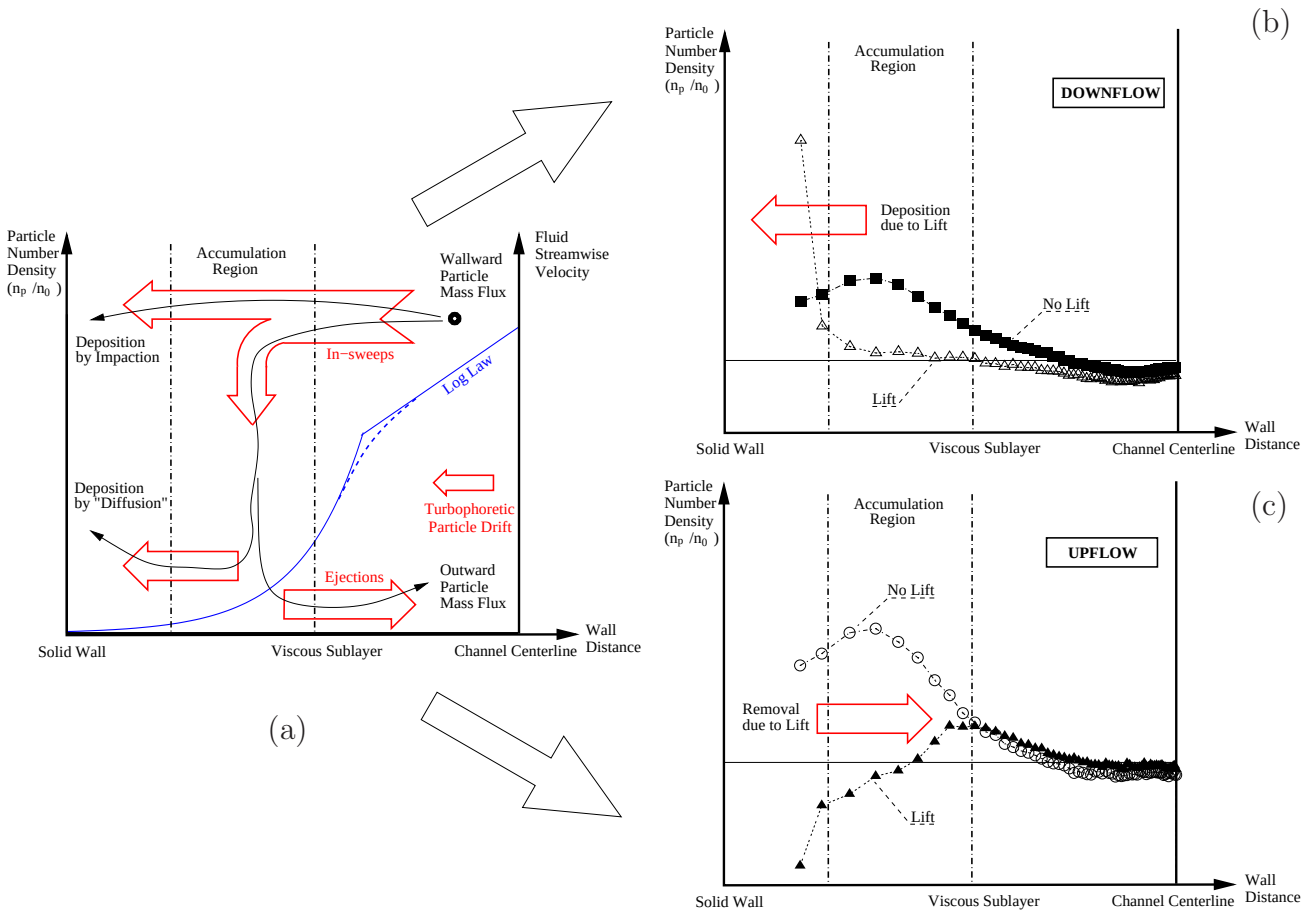

Figure 14 - “Influence of gravity and lift...” - Marchioli et al.

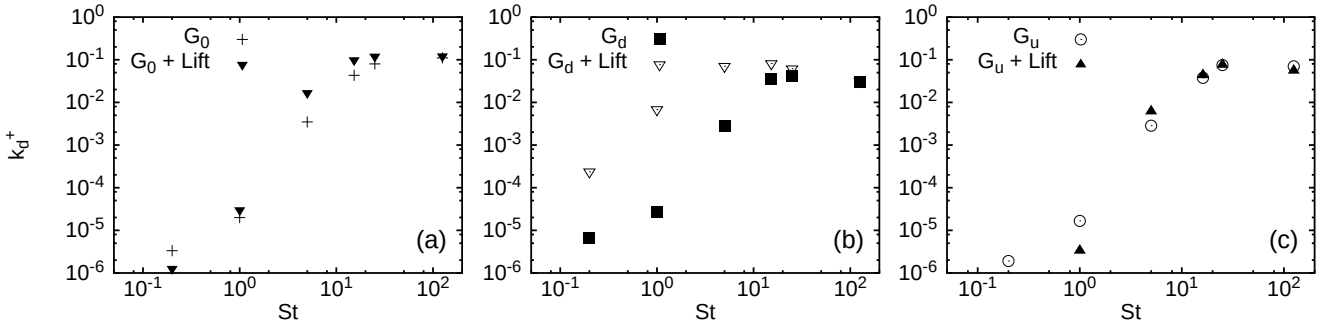

Figure 15 - "Influence of gravity and lift..." - Marchioli et al.